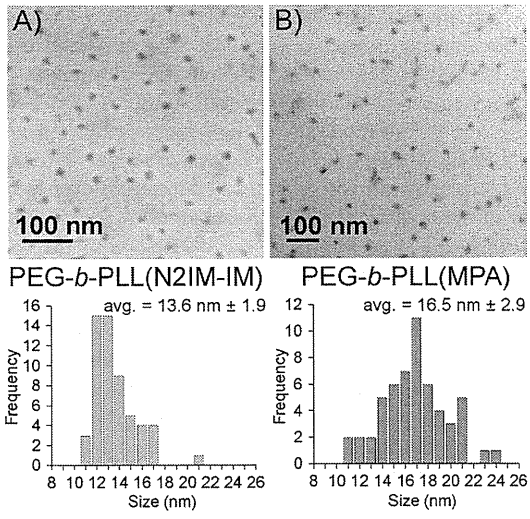

Figure 4. TEM images showing the morphology of cross-linked micelles. (A) PEG-*b*-PLL(N2IM-IM)/siRNA micelles, 80K magnification. (B) PEG-*b*-PLL(MPA) micelles, 50K magnification. The resulting size histograms from measuring the uranyl acetate stained micelle cores are shown below each image.

measurements. Addition of excess PEG-*b*-PLL(MPA) to the complexation mixture resulted in complete recovery of fluorescence intensity, indicating that the micelle structure was not maintained at high polymer/siRNA ratios. However, complexation of Cy3 siRNA with PEG-*b*-PLL(N2IM-IM) resulted in fluorescence quenching at polymer/siRNA ratio of ~1.8 and quenching was maintained up to the polymer/siRNA ratio of 7.6, indicating that polymer/siRNA complexes were unaffected by excess block copolymer. This result corroborates well with light scattering observations where the SLI of solutions prepared with PEG-*b*-PLL(MPA) and siRNA decreased at polymer:siRNA molar ratios greater than ~1.4 (showing micelle dissociation), whereas complexation solutions prepared with PEG-*b*-PLL(N2IM-IM) never exhibited a decrease in SLI up to the polymer/siRNA molar ratio of 7.6 (showing micelle structure is maintained).

In Vitro Micelle Stability. Cross-linked micelle stability was determined as a function of NaCl concentration in the presence or absence of the disulfide reducing agent DTT (Figure 3D). Increased NaCl concentration is expected to interfere with the ionic interactions between cationic polymer and siRNA, thus, disrupting micelle structures. This experiment was not intended to mimic biological conditions, but as a reference, the biological NaCl concentration is ~150 mM. In general, micelles prepared with siRNA and PEG-*b*-PLL(N2IM-IM) were more stable than those prepared with PEG-*b*-PLL(MPA). In the absence of DTT, micelles prepared with PEG-*b*-PLL(N2IM-IM) remained stable up to 600 mM NaCl, whereas micelles prepared with PEG-*b*-PLL(MPA) showed a significant decrease in SLI at 600 mM NaCl. Addition of DTT to the micelle solution resulted in an ~20% decrease in SLI at 600 mM NaCl for PEG-*b*-PLL(N2IM-IM), while the SLI of PEG-*b*-PLL(MPA) micelle solutions decreased to a greater extent (~30−50%) upon disulfide reduction at both 300 and 600 mM NaCl.

Micelle Morphology. Direct observation of cross-linked micelles by TEM showed uniform spherical structures less than 50 nm in size (Figure 4). The dark spheres in the TEM images

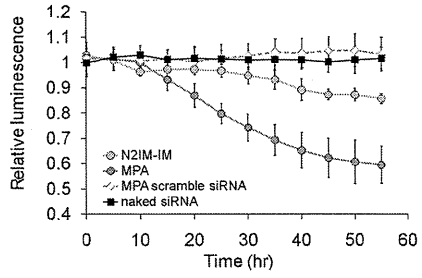

Figure 5. In vitro gene knockdown of luciferase in B16F10-luc cells. SiRNA was incorporated within cross-linked micelles prepared with PEG-*b*-PLL(X) (X = N2IM-IM or MPA) and introduced to cells at 200 nM siRNA. Data is presented as the ratio of treated sample luminescence to nontreated controls ± the standard deviation, $n = 4$.

correspond to the micelle core, as uranyl acetate specifically stains nucleic acids. Micelle core diameters were found to be 13.6 nm for PEG-*b*-PLL(N2IM-IM)/siRNA and 16.5 nm for PEG-*b*-PLL(MPA)/siRNA, both with narrow size distribution.

In Vitro Gene Silencing. The ability of micelles to deliver and release antiluciferase siRNA aimed to inhibit luciferase expression was determined in B16F10 murine melanoma cells stably expressing luciferase. In vitro gene silencing was highest when siRNA was administered encapsulated within micelles prepared with PEG-*b*-PLL(MPA), as shown in Figure 5. PEG-*b*-PLL(MPA)/siRNA micelle treated cells showed a modest (~40%) decrease in luminescence between 10 and 55 h, while PEG-*b*-PLL(N2IM-IM)/siRNA micelles showed a smaller (~12%) decrease in luminescence between 25 and 55 h. No cytotoxicity was observed for PEG-*b*-PLL(N2IM-IM)/siRNA or PEG-*b*-PLL(MPA)/siRNA micelles at siRNA concentrations up to 1000 nM, showing that luciferace knockdown was not due to reduced cell metabolism as a result of micelle introduction (see Supporting Information). Negligible luciferase knockdown was observed for naked siRNA or PEG-*b*-PLL(MPA)/siRNA micelles containing scramble siRNA, indicating that encapsulation within a micelle carrier is essential and also that the gene silencing was due to the siRNA effect and not due to the polymer used for micelle formation. No gene silencing was observed for PEG-*b*-PLL/siRNA micelles prepared at polymer/siRNA molar ratio of 1.2 (Table 1).

In Vivo Micelle Stability. Micelle behavior in the bloodstream was observed in mouse ear lobe dermis following I.V. injection. Naked siRNA was rapidly removed from the bloodstream (Figure 6A), with a half-life of approximately 3 min. Blood circulation time was improved by incorporating siRNA into disulfide-cross-linked micelle carriers, as the half-life increased to ~6 min for micelles prepared with PEG-*b*-PLL(MPA) and ~10 min for micelles prepared with PEG-*b*-PLL(N2IM-IM). Cy5 fluorescence intensity remained high for the first ~2 min for both disulfide-cross-linked micelle formulations but then rapidly decreased for PEG-*b*-PLL(MPA), with a profile similar to naked siRNA. The difference in blood vessel retention is clearly seen in Figure 6C, where Cy5 fluorescence remained high for PEG-*b*-PLL(N2IM-IM)/siRNA micelles after 10 min. No aggregates were visible in the bloodstream for any of the formulations following injection.

Extravasation of Cy5 into the surrounding skin tissue was apparent for naked siRNA and PEG-*b*-PLL(MPA)/siRNA micelles (Figure 6B). Extravasation is expected to occur only for low molecular weight species and, thus, indicates dissociation of the

micelles and possibly degradation of siRNA. Cy5 fluorescence increased in the tissue region more rapidly for PEG-*b*-PLL-(MPA)/siRNA micelles compared to PEG-*b*-PLL(N2IM-IM)/siRNA micelles. Tissue fluorescence for PEG-*b*-PLL(N2IM-IM)/siRNA micelles slowly increased over the 60 min observation period and never peaked (Figure 6B).

DISCUSSION

The focus of this work was to better understand the mechanism of polyion complex micelle formation between PEG-*b*-PLL(N2IM-IM) and siRNA, and also to observe the effects of polymer structure on micelle properties. Interest regarding the mechanism of micelle formation between PEG-*b*-PLL(N2IM-IM) and siRNA was sparked by observations from our previous work which showed that the optimal molar ratio of polymer/siRNA for micelle formation increased with increased IM content in the block copolymer. Further consultation with the literature suggested that the observed complexation behavior could be due to the tendency of 1-(4-mercaptobutyl) amidine groups initially formed following reaction of primary amines with 2-IT to cyclize and form N-substituted 2-iminothiolane moieties. The mechanism proposed for N-substituted 2-iminothiolane formation is shown in Figure 7, reproduced from the work of Mokotoff et al. and Singh et al.[16,17] These authors showed that reaction of primary amines with 2-IT resulted in the formation of linear 1-(4-mercaptobutyl) amidine functional groups initially but this species quickly disappeared along with concurrent appearance of cyclic N-substituted 2-iminothiolane structures. This behavior was also observed following the reaction of glucosamine with 2-IT, and the N-substituted 2-iminothiolane structure was confirmed by mass spectrometry.[26] Formation of the N-substituted 2-iminothiolane rings is rapid at room temperature and slightly basic pH, with half-lives of the initially formed 1-(4-mercaptobutyl) amidine ~0.5−3 h, depending on the pK_a of the amine nucleophile used for reaction with 2-IT. Specifically, the half-life of 1-(4-mercaptobutyl) amidines formed by reaction of 2-IT with amines having a pK_a of 9.3−9.8 (which is similar to the pK_a of lysine amines (~10) used for reaction with 2-IT in this study) is 1.8−2.8 h at pH 8, 25 °C.

Formation of the N-substituted 2-iminothiolane derivative in PEG-*b*-PLL(N2IM-IM) results in a five-membered ring structure. Thus, an appropriate amidination reagent must produce a mercaptoalkyl amidine not capable of ring formation. The chemistry contained in DTBP results in a formation of a 1-(3-mercaptopropyl) amidine group that contains only two carbons between the amidine and thiol and will not recyclize due to the instability of a four-membered ring. Modification of PEG-*b*-PLL with DTBP provided a convenient and stable structure for comparison with PEG-*b*-PLL(N2IM-IM).

^{1}H NMR analysis of PEG-*b*-PLL(N2IM-IM) confirmed that nearly all lysine amines reacted with 2-IT and also provided direct evidence that both cyclic N-substituted 2-iminothiolane and linear 1-(4-mercaptobutyl) amidine groups were present in the product (Figure 2). Generation of the N-substituted 2-iminothiolane has been reported to produce a small upfield shift (~0.2 ppm) of protons adjacent to the imine nitrogen in the ^{1}H NMR spectra of small molecules, and this small shift was also observed in the ^{1}H NMR spectrum of PEG-*b*-PLL(N2IM-IM).[16] The main peak at 3.25 ppm corresponds to lysine ε-CH_2 protons adjacent to N-substituted 2-iminothiolane containing side chains and the shoulder at 3.4 ppm corresponds to lysine ε-CH_2 protons adjacent to 1-(4-mercaptobutyl) amidine containing side chains. Estimation of the ratio of the two side chain structures from

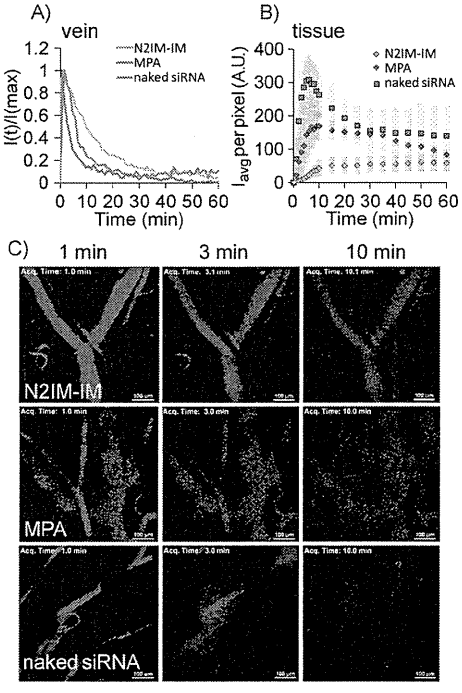

Figure 6. Behavior of siRNA incorporating micelles prepared with PEG-*b*-PLL(X) (X = N2IM-IM or MPA) following intravenous injection. (A) Residence time of Cy5 in the bloodstream normalized to the maximum observed intensity. (B) Cy5 fluorescence in the extravascular skin tissue, each data point represents the mean value ± the standard deviation of four regions of interest. (C) Snapshots of ear lobe dermis at 1, 3, and 10 min with Cy5 fluorescence shown as red. The scale bar represents 100 μm in each image. Representative data from one mouse for each sample is shown in A−C.

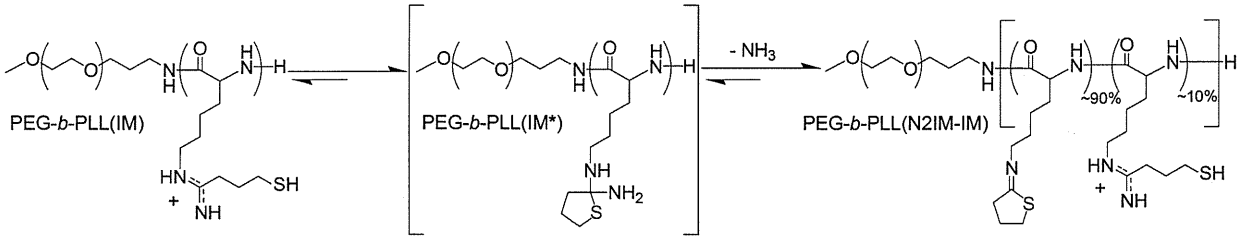

Figure 7. Intramolecular rearrangement of 1-(4-mercaptobutyl) amidine groups in PEG-*b*-PLL(IM) into N-substituted 2-iminothiolane moieties in PEG-*b*-PLL(N2IM-IM) via a tetrahedral intermediate structure. Adopted from Singh et al. and Mokotoff et al. (refs 16 and 17). Residual unmodified lysines are not shown in the chemical structures.

integration values showed that the N-substituted 2-iminothiolane ring is the predominant product following reaction with 2-IT (~75%). It should be noted that reaction of PEG-*b*-PLL with 1 molar equiv of 2-IT resulted in only ~60% conversion of lysine amines despite long (18 h) reaction time (data not shown). Reaction with at least a 2-fold excess of 2-IT is essential to achieve ~100% modification of lysine primary amines under the conditions described here. This is likely due to ammonia generated upon formation of N-substituted 2-iminothiolane rings competing for reaction with 2-IT and thus decreasing lysine amine conversion.

In our previous report, we obtained a product that did not show any N-substituted 2-iminothiolane functionality in the ^{1}H NMR spectrum of isolated polymer product, even at high lysine conversion (see Supporting Information). However, the siRNA complexation behavior at pH 7.4 was nearly identical between the PEG-*b*-PLL(IM) obtained in our previous report and the PEG-*b*-PLL(N2IM-IM) obtained in the current study. We found that treatment of PEG-*b*-PLL(IM) from the previous study with DTT at pH 7.4, and subsequent purification by dialysis, resulted in formation of the N-substituted 2-iminothiolane structures observed in this work (see Supporting Information). Thus, even if N-substituted 2-iminothiolane structures are not observed in the ^{1}H NMR spectrum of product obtained following reaction of PEG-*b*-PLL with 2-IT (at amounts targeting complete conversion of lysines), the ring structures will form upon reduction with DTT in aqueous buffer at pH 7.4. This seems reasonable if the isolated product contains a high degree of disulfide cross-linking, which would prevent the formation of N-substituted 2-iminothiolane rings. Disulfide formation during the reaction of PEG-*b*-PLL with 2-IT is likely why a residual amount of 1-(4-mercaptobutyl) amidine functionality is observed in the polymer product obtained in this study. It should be noted, however, that the structure of functional groups contained in PEG-*b*-PLL lysine side chains following reaction with lower molar ratios of 2-IT may be more complicated. Residual unmodified lysine amines can react with the N2IM structure to generate N,N′-disubstituted amidines, resulting in cross-linked (inter- or intramolecular) lysine side chains.[27] Thus, for simplicity, we targeted complete conversion of lysine amines with 2-IT in this study.

Formation of the N-substituted 2-iminothiolane derivative in PEG-*b*-PLL(N2IM-IM) product was also evidenced by analysis of free thiol content using Ellman's assay, as this cyclic moiety lacks sulfhydryl groups. Free thiol content was much lower for PEG-*b*-PLL(N2IM-IM) compared to PEG-*b*-PLL(MPA), confirming that the majority of modified lysines contained closed ring structures (Table 1). However, a finite amount (~10% of original lysine side chains) of free thiol was detected in PEG-*b*-PLL(N2IM-IM). This residual thiol content allows for the desired ability to form disulfide cross-links in the core of micelles prepared with PEG-*b*-PLL(N2IM-IM) and siRNA.

Polymeric micelles formed spontaneously upon mixing polymer and siRNA solutions in HEPES buffer (pH 7.4) at room temperature (22 °C). Complexation of block copolymer with siRNA was expressed as a function of the molar ratio of polymer/siRNA. We chose this format because of the complexity of the PEG-*b*-PLL(N2IM-IM) side chain structure, which makes exact definition of charge ratio difficult. Another method commonly used to express the polycation/nucleic acid ratio is N/P ratio. In this case, N typically represents the molar equivalent of amines (+ charge) and P represents the molar equivalents of siRNA phosphates (− charge). For polycations used in this study, the polymer/siRNA molar ratio is nearly interchangeable with N/P ratio if the charge is retained (i.e., PEG-*b*-PLL(MPA)), as the GL3 siRNA carries a net charge of (−) 40 and the PLL segment in the polycation block of PEG-*b*-PLL contains 46 units. This degree of polymerization for PLL was targeted so that one polymer chain neutralizes the charge of one siRNA molecule.

In general, modification of PEG-*b*-PLL with either 2-IT or DTBP improved the quality (controlled size and PDI) of micelles formed with siRNA. PEG-*b*-PLL alone formed large particles (~200 nm, PDI = 0.4) with siRNA near stoichiometric molar ratios (Table 1.). Micelle formation behavior between PEG-*b*-PLL(N2IM-IM) or PEG-*b*-PLL(MPA) and siRNA at pH 7.4 was markedly different. PEG-*b*-PLL(N2IM-IM) formed micelles over a broader range of polymer/siRNA molar ratios (~2−7.6) while micelles formed with PEG-*b*-PLL(MPA) only near stoichiometric molar ratios, with light scattering and fluorescence quenching results in good agreement (Figure 3A and 3C). Micelles formed at the polymer/siRNA molar ratio corresponding to the highest SLI value for both polymers were narrowly dispersed spherical structures as evidenced by the low PDI value obtained in DLS measurement (Table 1) and also by direct TEM observation (Figure 4). Excess polycation inhibited micelle formation in the case of PEG-*b*-PLL(MPA), as the SLI decreased and Cy3-siRNA fluorescence recovered at polymer/siRNA molar ratios above ~1.4 (Figure 3A,C). PEG-*b*-PLL(MPA) retains positive charge due to basic amidine groups (pK_a~11−12) and rearrangement of side chains into N-substituted 2-iminothiolane structures with a lower pK_a is prevented due to the shorter methylene spacer between the amidine and thiol.[28] The fact that micelles remain present in complexation mixtures containing a molar excess of PEG-*b*-PLL(N2IM-IM) suggests that this polymer is less charged than PEG-*b*-PLL(MPA), which is expected due to the prevalence of imines with a lower pK_a. Residual 1-(4-mercaptobutyl) amidine groups (which contain amidine functionality and thus positive charge) as well as unreacted lysine amines in PEG-*b*-PLL(N2IM-IM) likely provide the driving force for polymer association with siRNA through long-range Coulombic interactions. After polymer chains assemble in close proximity, additional short-range nonionic interactions (van der Waals, dipole−dipole, H-bonding) may occur to further stabilize the structure. When the residual charge of PEG-*b*-PLL(N2IM-IM) is considered (~5% unreacted lysines determined by ^{1}H NMR and 11% residual 1-(4-mercaptobutyl) amidines determined by Ellman's assay), a ± charge ratio of ~1.4 is calculated at the polymer/siRNA molar ratio of 7.6, where maximum SLI is observed. Assuming that all modified PLL side chains are charged in PEG-*b*-PLL(MPA), the polymer/siRNA molar ratio that resulted in maximum SLI corresponds to a ± ratio of 1.3. Thus, the ± charge ratio corresponding to maximum SLI were nearly the same for both PEG-*b*-PLL(N2IM-IM) and PEG-*b*-PLL(MPA) polymers at pH 7.4.

The effect of N-substituted 2-iminothiolane ring structures on block copolymer complexation with siRNA was confirmed by lowering the pH of complexation solutions. Formation of N-substituted 2-iminothiolane groups results in the loss of highly basic amidine groups and concurrent formation of imines of lower pK_a. For example, the pK_a value reported for an imine group contained in a N-substituted 2-iminothiolane formed by reaction of 2-IT with ethanolamine is reported as 6.7, which would result in a drastic loss of charge at pH 7.4 compared to the parent amidine.[16] At acidic complexation conditions

PEG-*b*-PLL(N2IM-IM) and PEG-*b*-PLL(MPA) behaved similarly, with micelles forming only at polymer/siRNA molar ratios near the stoichiometric region (Figure 3B). At pH 5.0, the imine groups of PEG-*b*-PLL(N2IM-IM) were protonated and, thus, cationic nature was restored, which in turn aligned the complexation behavior to that observed with PEG-*b*-PLL(MPA). Interestingly, although protonation of imines altered micelle formation behavior between PEG-*b*-PLL(N2IM-IM) and siRNA, incubation of cross-linked micelles (following disulfide reduction at pH 7.4) at pH 4.0 did not disrupt the micelle structure even at 150 mM NaCl (see Supporting Information). This treatment resulted in micelle swelling, but not micelle disruption.

Results with PEG-*b*-PLL(MPA) as well as protonated PEG-*b*-PLL(N2IM-IM) suggest that excess polycation disrupts micelle formation between block copolymers and siRNA. In the case of PEG-*b*-PLL(N2IM-IM), reduced polymer charge upon formation of N-substituted 2-iminothiolane rings likely reduced electrostatic repulsion between polymer chains and also competition for siRNAs, allowing more polymer to associate with micelle structures. Additionally, PEG-*b*-PLL(N2IM-IM) exhibited maximum fluorescence quenching at a lower polymer/siRNA molar ratio than that corresponding to the maximum SLI value (~7.6) and quenching was maintained over the entire range of polymer concentrations tested. This suggests that the polymer significantly interacts with siRNA at polymer/siRNA molar ratios ≥ 1.8, as evidenced by the change in the Cy3 microenvironment leading to quenching. However, polymer association is not complete until polymer:siRNA molar ratios of ~7.6, where maximum SLI was observed. This is consistent with our previous gel retardation studies of micelles prepared with siRNA and PEG-*b*-PLL(N2IM-IM), where siRNA did not enter the gel for complexation solutions prepared at polymer/siRNA ratios >2.7.[14]

Micelle *z*-average diameters measured by DLS and micelle core sizes determined by TEM were in good agreement, and the sizes obtained were similar for both PEG-*b*-PLL(N2IM-IM) and PEG-*b*-PLL(MPA) (Table 1 and Figure 4). Low PDI values obtained by DLS measurement of polymer/siRNA assemblies suggests that spherical structures formed, which was confirmed by direct TEM observation of cross-linked micelles. As expected, micelle diameters determined by DLS analysis were larger than the core size of micelles determined from the TEM images. However, the determined size of micelle cores by TEM corroborated well with whole micelle size values observed by DLS, considering the size of PEG and assuming a core−shell micelle structure. The radius of gyration (R_g) of PEG 12K in water is 4.68 nm; thus, the tethered PEG chain height is 9.36 nm ($2 \times R_g$) in the so-called mushroom or random coil conformation.[29,30] Addition of the PEG segment length to the measured micelle core size obtained from TEM images results in a calculated diameter of 32.3 nm for PEG-*b*-PLL(N2IM-IM)/siRNA micelles and 35.2 nm for PEG-*b*-PLL(MPA)/siRNA micelles, which are less than the *z*-average values reported in Table 1. Conversion of DLS data to number average diameters directly from the size distribution histogram generated from the ZetaSizer software resulted in a calculated diameter of 32.0 ± 2.37 nm for PEG-*b*-PLL(N2IM-IM)/siRNA micelles and 32.4 nm ±1.3 nm for PEG-*b*-PLL(MPA)/siRNA micelles, which is in excellent agreement with calculated diameters from TEM images (see Supporting Information). Micelle core diameters measured from TEM imaging were smaller for PEG-*b*-PLL(N2IM-IM)/siRNA, while the whole micelle diameter measured by DLS was the same for both PEG-*b*-PLL(N2IM-IM) and PEG-*b*-PLL(MPA). This suggests that the PEG layer may be thicker in PEG-*b*-PLL(N2IM-IM)/siRNA micelles, where PEG chains become more elongated on the micelle surface due to the close proximity of other chains. This seems reasonable as more polymer may be associating with PEG-*b*-PLL(N2IM-IM)/siRNA micelles, which form in the presence of ~7.6 times molar excess of polymer. Altogether, micelle characterization by both DLS and TEM further support that core−shell micelle structures are formed upon association of polymer with siRNA at the polymer:siRNA molar ratio corresponding to maximum SLI.

Modification of PEG-*b*-PLL with 2-IT or DTBP increased the stability of PIC micelles formed with siRNA as evidenced by the maintenance of micelle structures formed with both block copolymers up to 300 mM NaCl (Figure 3D), whereas non-cross-linked assemblies (but not necessarily individual polyion complexes) formed between siRNA and PEG-*b*-PLL nearly completely dissociate in 150 mM NaCl.[14] However, PEG-*b*-PLL(N2IM-IM)/siRNA micelles were ultimately more stable than PEG-*b*-PLL(MPA)/siRNA micelles at high NaCl concentration (600 mM). This suggests that nonionic interactions, such as van der Waals, ion-dipole, or H-bonding (via imine nitrogens) may also contribute to micelle stability. Incubation of PEG-*b*-PLL(N2IM-IM)/siRNA micelles in a high ionic strength solution under reductive conditions resulted in disruption of micelle structures (~20% decrease in SLI compared to nonreductive conditions), showing that disulfide cross-links did in fact contribute to micelle stability.

For PEG-*b*-PLL(MPA), dissociation of micelles at high NaCl concentration in the absence of DTT suggests that disulfide cross-linking alone did not provide the same stability provided by PEG-*b*-PLL(N2IM-IM), which had a much lower thiol content and disulfide formation efficiency in the micelle core. However, the degree of intermolecular vs intramolecular disulfide cross-linking in PEG-*b*-PLL(MPA)/siRNA micelles is unknown, and only the former would result in increased micelle stability in the absence of disulfide reducing agents. Micelles formed with PEG-*b*-PLL(MPA) were more sensitive to dissociation in the presence of DTT, indicating that disulfide cross-linking was more critical to improving the stability of micelles prepared solely from electrostatic interactions.

In vitro gene silencing activity of siRNA was improved upon encapsulation within polymeric micelle carriers prepared from PEG-*b*-PLL(N2IM-IM) or PEG-*b*-PLL(MPA), as no gene silencing was observed for naked siRNA or PEG-*b*-PLL particles (Figure 5 and Table 1). Gene silencing was highest for PEG-*b*-PLL(MPA)/siRNA micelles, which may be attributed to higher sensitivity to disulfide reduction. PEG-*b*-PLL(MPA)/siRNA micelles likely dissociate more readily once internalized into cells, thus, releasing the siRNA cargo. This is consistent with the observed difference in lag time before gene silencing, where PEG-*b*-PLL(MPA)/siRNA micelles showed gene silencing after only 10 h and PEG-*b*-PLL(N2IM-IM)/siRNA micelles showed gene silencing after 25 h. More stable PEG-*b*-PLL(N2IM-IM) micelles likely dissociate and release siRNA more slowly, thus, requiring more time before gene knockdown is observed. Nonetheless, the fact that gene silencing was observed after 55 h of incubation indicates that both micelle structures were effective at protecting siRNA from degradation into inactive fragments within the cell culture medium or off-target sites within the subcellular environment.

One of our goals regarding development of a siRNA delivery system is to produce a carrier that has prolonged residence time

in the bloodstream, allowing the carrier to be administered by I.V. injection. Polymer/siRNA micelle structures obtained in this study are particularly attractive candidates for cancer treatment by I.V. injection as they are large enough to escape rapid renal filtration (~ 10 nm cutoff) but small enough (<100 nm) to gain tumor mass accumulation by the enhanced permeability and retention (EPR) effect.[31,32] Thus, we investigated the blood circulation time of micelles prepared in this work. In order to have prolonged blood circulation the carrier must not interact with blood components (leading to aggregation or micelle dissociation) and must also remain intact to protect siRNA from premature release and degradation. Blood circulation results clearly identify that micelles prepared with PEG-*b*-PLL(N2IM-IM) and siRNA remain in the bloodstream longer than any other formulation tested (Figure 6A). Micelles prepared with PEG-*b*-PLL(MPA) provided some improvement in blood residence time compared to naked siRNA and PEG-*b*-PLL/siRNA particles. This result suggests that even a high degree of disulfide cross-linking was insufficient to greatly prolong residence time in the bloodstream. However, although disulfide formation efficiency was high for PEG-*b*-PLL(MPA)/siRNA micelles, the amount of intermolecular cross-linking is unknown. A longer spacer between the amidine and thiol in modified PLL side-chains may further improve micelle stability and blood residence time.

Improved blood circulation for PEG-*b*-PLL(N2IM-IM)/siRNA micelles may not be solely linked to micelle stability. As mentioned previously, the PEG density is likely higher for micelles formed with PEG-*b*-PLL(N2IM-IM) than those prepared with PEG-*b*-PLL(MPA) as the former were prepared at a higher molar ratio of polymer. Higher PEG density may further reduce nonspecific interactions of micelles with blood components leading to longer circulation time. The impact of PEG density on stability in the blood compartment is beyond the scope of this study but we hope to clarify this in the future. Furthermore, the lower charge density of PEG-*b*-PLL(N2IM-IM) likely results in diffuse charges in the micelle core which in turn could reduce interactions with charged (mainly anionic) components in the bloodstream.

In addition to providing the longest blood circulation time, micelles prepared with PEG-*b*-PLL(N2IM-IM) also showed the lowest increase in tissue fluorescence outside of blood vessels. Extravasation into surrounding tissues suggests that micelle structures dissociated and fluorescent labeled siRNA was released and possibly degraded, producing small fragments of siRNA with high tissue permeability. We have previously observed such effects with fluorescein and fluorescein-labeled dextrans. In that study, we observed that free dye and dye-labeled dextrans lower than ~10 kDa quickly entered the tissue following I.V. injection, whereas higher MW dye-labeled dextrans did not.[21] Thus reduced migration of Cy5 fluorescence into the tissue region surrounding blood vessels in the case of PEG-*b*-PLL(N2IM-IM)/siRNA micelles provides further evidence that micelles remained intact in the bloodstream.

In summary, we found that a highly charged cationic block copolymer was not necessary to form micellar structures with siRNA. PEG-*b*-PLL(N2IM-IM) formed micelles with siRNA despite loss of a large percentage of charged amidine groups. This block copolymer likely retained enough residual charge to interact with siRNA and assemble into higher-ordered micellar structures but not so much charge as to electrostatically repel itself at high polymer concentrations. The unique association behavior of PEG-*b*-PLL(N2IM-IM) and siRNA represents a nontraditional PIC assembly where the polycation contains low charge density and micelles form in the presence of excess block copolymer. In this regard, PEG-*b*-PLL(N2IM-IM)/siRNA micelles are attractive from a practical point of view because micelle formation is less sensitive to slight variations in polymer concentration. In contrast, strongly charged PEG-*b*-PLL(MPA) cationic block copolymer showed very sensitive micelle formation behavior with siRNA and excess polycation inhibited micelle assembly. Inhibition of micelle formation was likely due to repulsion of charged polymer chains and increased competition with siRNAs. As a result, preparation of micelles with PEG-*b*-PLL(MPA) and siRNA required careful control of polymer and siRNA mixing ratios.

Covalent disulfide cross-linking is expected to improve micelle stability compared to particles prepared from unmodified PEG-*b*-PLL, but a high thiol-content block copolymer did not produce the most stable micelle structure in this work. Micelles prepared from polymer comprising relatively low free thiol content were more resistant to dissociation in vitro and also exhibited longer residence time in the bloodstream in vivo. The possibility of noncovalent interactions between polymer chains in addition to covalent disulfide cross-linking greatly improved micelle stability. Improved micelle stability came at a performance cost, as noncovalent polymer interactions in addition to covalent disulfide cross-links reduced the sensitivity of micelles to disruption under disulfide reducing conditions. Increased stability and reduced sensitivity to disulfide reduction were likely responsible for the increased lag-time observed for the onset of gene silencing in cell culture experiments. On the other hand, the benefit of preparing stable micelles with high polymer content was realized in vivo. Micelles prepared with PEG-*b*-PLL(N2IM-IM) exhibited longer blood circulation, which is necessary for I.V. administration of siRNA delivery systems. Thus, the chemistry contained in the block copolymer must be carefully controlled to produce effective siRNA carriers on the cellular and whole organism level.

Understanding the mechanisms that govern the assembly and stability of nanoparticles is crucial for improvements of their design. The findings of this work may be further generalized in the sense that "soft" polycations containing less positive charge and "hard" polycations with high charge density differ in their complexation behavior with siRNA. While interactions between polyelectrolytes can provide the driving force for particle assembly, the stability of the resulting polyplex may be further enhanced by contributions from nonionic interactions in addition to covalent cross-links to form more robust structures. Formation of micelle structures between polymers and siRNA may be more sensitive to the chemistries contained in the polymer component than large polyanions such as plasmid DNA (pDNA). siRNA is much smaller than pDNA and cannot condense and adopt different conformations in response to excess polycation. Instead, siRNA can simply dissociate from the polyion complex due to the increased mobility of a shorter polyanion. Preparation of stable siRNA polymeric micelle nanocarriers is hinged on a delicate balance of chemistries contained in the polymer component.

CONCLUSIONS

In this work, we found that a high degree of PEG-*b*-PLL modification with 2-iminothiolane resulted in the formation of N-substituted 2-iminothiolane structures in the majority of reacted lysine side chains. This chemistry reduced the polymer charge density at pH 7.4, which in turn shifted the optimal conditions of micelle formation to favor higher molar ratios of

polymer/siRNA compared to a highly charged block copolymer. Despite lower free thiol content and disulfide cross-linking efficiency, micelles formed with PEG-*b*-PLL(N2IM-IM) and siRNA were more stable in buffer and in the bloodstream compared to those formed with PEG-*b*-PLL(MPA) and siRNA. These results highlight the importance of nonionic and noncovalent interactions toward the stability of micelles formed between siRNA and block copolymers. However, higher micelle stability and loss of sensitivity to disulfide reducing conditions resulted in lower siRNA activity on the cellular level; thus, reversible micelle stability is critical to achieve high gene silencing at the target site. The siRNA encapsulating micelles described in this work are promising candidates as carriers for siRNA delivery applications and our efforts to correlate micelle properties with in vitro and in vivo efficacy are ongoing.

■ ASSOCIATED CONTENT

Supporting Information. Figures showing (1) a summary of scattered light intensity, size, and PDI of micelles (non-cross-linked) contained in PEG-*b*-PLL(N2IM-IM)/siRNA solutions at various polymer concentrations, (2) scattered light intensity, size, and PDI of PEG-*b*-PLL(N2IM-IM) polymer solutions at pH 7.4 and 4.0, (3) scattered light intensity of cross-linked PEG-*b*-PLL(N2IM-IM) micelles at pH 7.4 and pH 4.0 at various micelle concentrations, (4) size distribution histograms of cross-linked micelles determined by DLS, (5) ^{1}H NMR analysis of PEG-*b*-PLL(IM) following reduction in DTT at pH 7.4, (6) cytotoxicity of polymer/siRNA micelles prepared with PEG-*b*-PLL(N2IM-IM) and PEG-*b*-PLL(MPA), and (7) blood circulation profile of cross-linked micelles in different mice (n = 2) are provided. This material is available free of charge via the Internet at http://pubs.acs.org.

■ AUTHOR INFORMATION

Corresponding Author

*Tel.: +81-3-5841-7138. Fax: +81-3-5841-7139. E-mail: kataoka@bmw.t.u-tokyo.ac.jp.

■ ACKNOWLEDGMENT

This research was financially supported by the Funding Program for World-Leading Innovative R&D in Science and Technology (FIRST), the Japan Society for the Promotion of Science (JSPS), and the Core Research Program for Evolutional Science and Technology (CREST) from the Japan Science and Technology Agency (JST).

■ REFERENCES

(1) Whitehead, K.; Langer, R.; Anderson, D. *Nat. Rev. Drug Discovery* **2009**, *8*, 129–138.
(2) Gary, D.; Puri, N.; Won, Y. *J. Controlled Release* **2007**, *121*, 64–73.
(3) Juliano, R.; Alam, M.; Dixit, V.; Kang, H. *Nucleic Acids Res.* **2008**, *36*, 4158–4171.
(4) Ai, H.; Jones, S.; Lvov, Y. *Cell Biochem. Biophys.* **2003**, *39*, 23–43.
(5) Hammond, P. *Adv. Mater.* **2004**, *16*, 1271–1293.
(6) Christie, R.; Nishiyama, N.; Kataoka, K. *Endocrinology* **2010**, *151*, 466–473.
(7) Wang, Y.; Angelatos, A.; Caruso, F. *Chem. Mater.* **2008**, *20*, 848–858.
(8) Mintzer, M.; Simanek, E. *Chem. Rev.* **2009**, *109*, 259–302.
(9) Meyer, M.; Philipp, A.; Oskuee, R.; Schmidt, C.; Wagner, E. *J. Am. Chem. Soc.* **2008**, *130*, 3272–3273.
(10) Lee, Y.; Miyata, K.; Oba, M.; Ishii, T.; Fukushima, S.; Han, M.; Koyama, H.; Nishiyama, N.; Kataoka, K. *Angew. Chem., Int. Ed.* **2008**, *47*, 5163–5166.
(11) Convertine, A.; Benoit, D.; Duvall, C.; Hoffman, A.; Stayton, P. *J. Controlled Release* **2009**, *133*, 221–229.
(12) Takae, S.; Miyata, K.; Oba, M.; Ishii, T.; Nishiyama, N.; Itaka, K.; Yamasaki, Y.; Koyama, H.; Kataoka, K. *J. Am. Chem. Soc.* **2008**, *130*, 6001–6009.
(13) Miyata, K.; Kakizawa, Y.; Nishiyama, N.; Harada, A.; Yamasaki, Y.; Koyama, H.; Kataoka, K. *J. Am. Chem. Soc.* **2004**, *126*, 2355–2361.
(14) Matsumoto, S.; Christie, R.; Nishiyama, N.; Miyata, K.; Ishii, A.; Oba, M.; Koyama, H.; Yamasaki, Y.; Kataoka, K. *Biomacromolecules* **2009**, *10*, 119–127.
(15) Meister, A.; Anderson, M. *Annu. Rev. Biochem.* **1983**, *52*, 711–760.
(16) Singh, R.; Kats, L.; Blattler, W.; Lambert, J. *Anal. Biochem.* **1996**, *236*, 114–125.
(17) Mokotoff, M.; Mocarski, Y.; Gentsch, B.; Miller, M.; Zhou, J.; Chen, J.; Ball, E. *J. Pept. Res.* **2001**, *57*, 383–389.
(18) Harada, A.; Kataoka, K. *Macromolecules* **1995**, *28*, 5294–5299.
(19) Ellman, G. *Arch. Biochem. Biophys.* **1959**, *82*, 70–77.
(20) Tam, J. P.; Wu, C. R.; Liu, W.; Zhang, J. W. *J. Am. Chem. Soc.* **1991**, *113*, 6657–6662.
(21) Matsumoto, Y.; Nomoto, T.; Cabral, H.; Matsumoto, Y.; Watanabe, S.; Christie, R. J.; Miyata, K.; Oba, M.; Ogura, T.; Yamasaki, Y.; Nishiyama, N.; Yamasoba, T.; Kataoka, K. *Biom. Opt. Express* **2010**, *1*, 1209–1216.
(22) Browne, D.; Kent, S. *Biochem. Biophys. Res. Commun.* **1975**, *67*, 126–132.
(23) Gruber, H.; Hahn, C.; Kada, G.; Riener, C.; Harms, G.; Ahrer, W.; Dax, T.; Knaus, H. *Bioconjugate Chem.* **2000**, *11*, 696–704.
(24) Berlier, J.; Rothe, A.; Buller, G.; Bradford, J.; Gray, D.; Filanoski, B.; Telford, W.; Yue, S.; Liu, J.; Cheung, C.; Chang, W.; Hirsch, J.; Beechem, J.; Haugland, R. *J. Histochem. Cytochem.* **2003**, *51*, 1699–1712.
(25) Anbazhagan, V.; Kathiravan, A.; Jhonsi, M.; Renganathan, R. *Z. Phys. Chem.* **2007**, *221*, 929–939.
(26) Kafedjiiski, K.; Krauland, A.; Hoffer, M.; Bernkop-Schnurch, A. *Biomaterials* **2005**, *26*, 819–826.
(27) Hahn, F.; Mullen, K.; Schepers, U. *Synlett* **2008**, *18*, 2785–2790.
(28) Koppel, I.; Koppel, J.; Leito, I.; Green, L. *J. Phys. Org. Chem.* **1996**, *9*, 265–268.
(29) Kawaguchi, S.; Imai, G.; Suzuki, J.; Miyahara, A.; Kitano, T. *Polymer* **1997**, *38*, 2885–2891.
(30) Kenausis, G.; Voros, J.; Elbert, D.; Huang, N.; Hofer, R.; Ruiz-Taylor, L.; Textor, M.; Hubbell, J.; Spencer, N. *J. Phys. Chem. B* **2000**, *104*, 3298–3309.
(31) Choi, H.; Liu, W.; Misra, P.; Tanaka, E.; Zimmer, J.; Ipe, B.; Bawendi, M.; Frangioni, J. *Nat. Biotechnol.* **2007**, *25*, 1165–1170.
(32) Maeda, H.; Wu, J.; Sawa, T.; Matsumura, Y.; Hori, K. *J. Controlled Release* **2000**, *65*, 271–284.

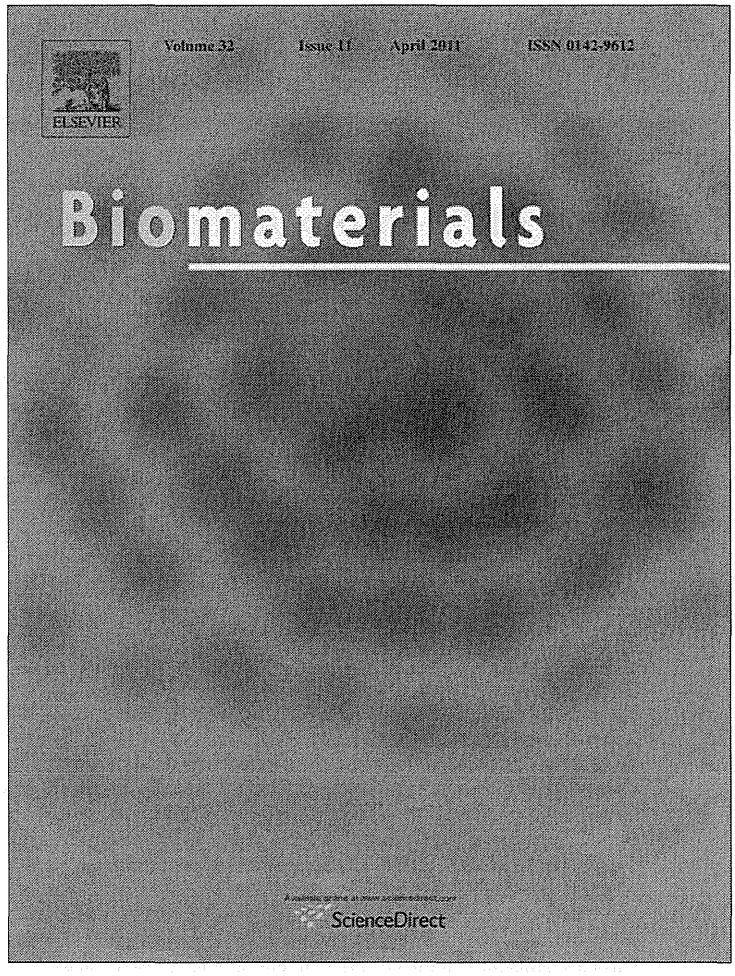

Biomaterials 32 (2011) 3106–3114

Contents lists available at ScienceDirect

Biomaterials

journal homepage: www.elsevier.com/locate/biomaterials

Enhanced endosomal escape of siRNA-incorporating hybrid nanoparticles from calcium phosphate and PEG-block charge-conversional polymer for efficient gene knockdown with negligible cytotoxicity

Frederico Pittella [a], Mingzhen Zhang [b,d], Yan Lee [b,e], Hyun J. Kim [b], Theofilus Tockary [b], Kensuke Osada [b], Takehiko Ishii [a], Kanjiro Miyata [c], Nobuhiro Nishiyama [c], Kazunori Kataoka [a,b,c,*]

[a] Department of Bioengineering, Graduate School of Engineering, The University of Tokyo, 7-3-1 Hongo, Bunkyo-ku, Tokyo 113-8656, Japan
[b] Department of Materials Engineering, Graduate School of Engineering, The University of Tokyo, 7-3-1 Hongo, Bunkyo-ku, Tokyo 113-8656, Japan
[c] Center for Disease Biology and Integrative Medicine, Graduate School of Medicine, The University of Tokyo, 7-3-1 Hongo, Bunkyo-ku, Tokyo 113-0033, Japan
[d] School of Ophthalmology and Optometry, Wenzhou Medical College, Wenzhou, Zhejiang 325027, PR China
[e] Department of Chemistry, College of Natural Science, Seoul National University, Seoul 151-747, Republic of Korea

ARTICLE INFO

Article history:
Received 4 December 2010
Accepted 31 December 2010
Available online 26 January 2011

Keywords:
Calcium phosphate nanoparticles
Endosomal escape
Vascular endothelial growth factor (VEGF)
siRNA
Charge-conversional polymer (CCP)
Poly(ethylene glycol) (PEG)

ABSTRACT

Development of safe and efficient short interfering RNA (siRNA) delivery system for RNA interference (RNAi)-based therapeutics is a current critical challenge in drug delivery field. The major barriers in siRNA delivery into the target cytoplasm are the fragility of siRNA in the body, the inefficient cellular uptake, and the acidic endosomal entrapment. To overcome these barriers, this study is presenting a hybrid nanocarrier system composed of calcium phosphate comprising the block copolymer of poly(ethylene glycol) (PEG) and charge-conversional polymer (CCP) as a siRNA vehicle. In these nanoparticles, the calcium phosphate forms a stable core to incorporate polyanions, siRNA and PEG–CCP. The synthesized PEG–CCP is a non-toxic endosomal escaping unit, which induces endosomal membrane destabilization by the produced polycation through degradation of the flanking *cis*-aconitylamide of CCP in acidic endosomes. The nanoparticles prepared by mixing of each component was confirmed to possess excellent siRNA-loading efficiency (~80% of dose), and to present relatively homogenous spherical shape with small size. With negligible cytotoxicity, the nanoparticles efficiently induced vascular endothelial growth factor (VEGF) mRNA knockdown (~80%) in pancreatic cancer cells (PanC-1). Confocal laser scanning microscopic observation revealed rapid endosomal escape of siRNA with the nanoparticles for the excellent mRNA knockdown. The results obtained demonstrate our hybrid nanoparticle as a promising candidate to develop siRNA therapy.

1. Introduction

Since the finding of RNA interference (RNAi) in 1998 [1], the scientific community has experienced the excitement to develop a new research field. Short interfering RNA (siRNA), which allows the cleavage of the complementary mRNA for the reduced protein production in mammalian cells, provided new perspectives for potential treatment of intractable and genetic related diseases [2]. With the decoding of the human genome [3–5], it has become possible to aim a great variety of genes involved in key pathways of physiopathologies. However, a safe and efficient delivery of siRNA into the target cytoplasm has still been a major challenge. Naked siRNAs are susceptible to enzymatic degradation in the body and also possess large size (~13 kDa) and anionic charges suppressing the penetration into cellular membrane [6], thus requiring carrier systems to overcome these barriers.

Calcium phosphate (CaP) precipitates were used as transfection reagents of viral DNA for the first time in early 1970s [7], as they are believed to be non-toxic based on homology to natural inorganic materials such as teeth and bones. Notably, CaP precipitates can bind and encapsulate polyanions/nucleic acids by an easy and inexpensive method to protect the nucleic acids from enzymatic degradation and to deliver into cells. However, one of their major limitations is the uncontrollable rapid growth of calcium phosphate crystal after preparation, resulting in the formation of large agglomerates (>μm) to appreciably reduce the transfection efficiency [8–10]. In this regard, our previous studies have addressed poly(ethylene glycol) (PEG)-coating of CaP precipitates utilizing PEG-polyanion block copolymers [9,11–14]. Hydrophilic and neutral PEG is widely known

* Corresponding author. Department of Bioengineering, Graduate School of Engineering, The University of Tokyo, 7-3-1 Hongo, Bunkyo-ku, Tokyo 113-8656, Japan.
E-mail address: kataoka@bmw.t.u-tokyo.ac.jp (K. Kataoka).

0142-9612/$ – see front matter © 2011 Elsevier Ltd. All rights reserved.
doi:10.1016/j.biomaterials.2010.12.057

to provide a nanoparticle with excellent colloidal stability as well as reduced protein adsorption and immunogenicity [15–17]. Indeed, the integration of PEG-block polyanions, such as poly(aspartic acid) (PAsp) [9,12], poly(methacryl acid) [13], and siRNA [14], into CaP precipitates led to the formation of size-controllable hybrid nanoparticles with PEG palisade, which appreciably facilitated the internalization of nucleic acids by cells.

Herein, we considered the next challenge in the CaP carriers as the endosomal escape, since they are usually internalized by cells though endocytosis pathway to be delivered into acidic endosome or lysosome, resulting in enzymatic degradation of the payload nucleic acids [18]. Toward the endosomal escape with polymeric materials, our previous studies have reported a cationic polyaspartamide with a 1,2-diaminoethane side chain (poly{*N*-[*N*′-(2-aminoethyl)-2-aminoethyl] aspartamide}, PAsp(DET)) to exert strong membrane destabilization selectively in acidic endosomal compartments for efficient endosomal escape with low cytotoxicity [19–22]. Note that PAsp(DET) possesses two unique advantages for its excellent transfection: 1) the pH-selective membrane destabilization based on the distinctive two step protonation behavior in the side chain, i.e., mono-protonated form with minimal membrane damages at neutral pH and di-protonated form exerting strong membrane disruption at acidic pH [20]; 2) the spontaneous biodegradability based on the selective backbone cleavage even under physiological conditions [21].

In this work, in order to improve the endosomal escape as well as the colloidal stability of CaP precipitates, a block copolymer of PEG and an endosomal escaping polymer was synthesized and integrated into the CaP nanoparticles incorporating siRNA. Indeed, we modified the flanking primary amines of PEG-PAsp(DET) with *cis*-aconitic anhydride [23,24] to convert the cationic charges to net negative ones with two carboxylates of the *cis*-aconityl moiety (PEG-poly{*N*-[*N*′-(*N*″-*cis*-aconityl-2-aminoethyl)-2-aminoethyl]aspartamide}, PEG-PAsp(DET-Aco)) for effective binding to CaP nanoparticles. Noteworthy, the prepared *cis*-aconitylamide shows high stability at neutral and basic pHs but it becomes cleavable at acidic pH to reproduce cationic PAsp(DET) from anionic PAsp(DET-Aco) in endosome/lysosome, which is termed the charge-conversional polymer [23–25]. The hybrid nanoparticle prepared from PEG-PAsp (DET-Aco), siRNA, and CaP does not contain inherent toxic materials, such as polycations, thereby leading to potentially lower toxicity compared to conventional polyplex carriers from polycations and siRNA. Thus, the nanoparticles prepared by simple mixing of each component were physicochemically and biologically characterized by the comparison with non-charge-conversional control polyanions to demonstrate the utility of our hybrid system from the PEG–charge-conversional polymer for siRNA delivery.

2. Material and methods

2.1. Materials

cis-Aconitic anhydride, tricarballylic acid, and Dulbecco's modified eagle's medium (DMEM) were purchased from Sigma–Aldrich (St. Louis, MO). α-Methoxy-ω-amino-poly(ethylene glycol) (MeO–PEG–NH_2) (M_w: 12,000) and β-benzyl-L-aspartate *N*-carboxyanhydride (BLA–NCA) were obtained from NOF Co, Inc. (Tokyo, Japan) and Chuo Kaseihin Co., Inc. (Tokyo, Japan), respectively. *N*-Methyl-2-pyrrolidone (NMP), diethylenetriamine (DET), dimethyl sulfoxide (DMSO), *N*,*N*-dimethylformamide (DMF), dichloromethane (DCM), and acetic anhydride were purchased from Tokyo Chemical Industry Co. Ltd. (Tokyo, Japan) or Nacalai Tesque (Tokyo, Japan), and used after a conventional distillation. Acetic acid, acetonitrile, acetone, diethyl ether, and hydrochloric acid were purchased from Wako Pure Chemical Industries Ltd. (Osaka, Japan). Fetal bovine serum (FBS) was purchased from Dainippon Sumitomo Pharma Co., Ltd. (Osaka, Japan). The primers for human actin and human VEGF were synthesized by Hokkaido System Science (Hokkaido, Japan) and the sequences are: CCAACCGCGAGAAGATGA (actin forward); CCAGAGGCGTACAGGGATAG (actin reverse); AGTGGTCCCAGGCTGCAC (VEGF forward); TCCATGAACTTCACCACTTCGT (VEGF reverse). All the siRNAs were synthesized by Hokkaido System Science (Hokkaido, Japan) and the sequences of VEGF siRNA (siVEGF) are: 5′-GGAGUACCCUGAUGAGAUCdTdT-3′ (sense); 5′-GAUCUCAUCAGGGUACUCCdTdT-3′ (antisense), and GL3 luciferase siRNA (siGL3) are: 5′-CUU ACG CUG AGU ACU UCG AdTdT-3′ (sense); 5′-UCG AAG UAC UCA GCG UAA GdTdT-3′ (antisense).

2.2. Synthesis of block copolymer with poly(ethylene glycol) and charge-conversional polymer (PEG–CCP) segments

2.2.1. Synthesis of poly(ethylene glycol)-b-poly{N-[N-(2-aminoethyl)-2-aminoethyl] aspartamide} (PEG-PAsp(DET))

PEG-PAsp(DET) was prepared as previously reported with slight modification [21]. Briefly, BLA–NCA (780 mg; 3.13 mmol) was dissolved in 0.7 mL of DMF, and then in 7.3 mL of DCM. The polymerization was initiated from the primary amino group of MeO–PEG–NH_2 (M_w = 12,000, 500 mg; 0.0417 mmol) to obtain PEG–PBLA (1100 mg) as a precursor. Size exclusion chromatography (SEC) was performed to determine the molecular weight distribution (M_w/M_n) of the obtained PEG–PBLA using a TOSOH HLC-8220 equipped with TSK gel columns (SuperAW4000 and SuperAW3000 × 2; eluent: NMP with 50 mM LiBr; flow rate: 0.3 mL min^{-1}; temperature: 40 °C) and an internal refractive index (RI) detector. The M_w/M_n was confirmed to be 1.07 from the SEC chart using PEG standards for the M_w calibration (data not shown). The degree of polymerization of PBLA in PEG–PBLA was determined to be 96 from the peak intensity ratio of the methylene protons of PEG (–OCH_2CH_2–, δ = 3.5 ppm) to the benzyl protons of PBLA ($C_6H_5CH_2$–, δ = 5.1 and 7.3 ppm) in the ^{1}H NMR measurement (data not shown). All of the NMR assays were performed using (3-(trimethylsilyl)-3,3,2,2-tetradeuteropropionic acid sodium salt d_4-TSPA) as an internal standard. Then, PEG–PBLA (100 mg) was dissolved in NMP (2 mL) and cooled at 5 °C. Diethylenetriamine (DET) (3 mL; 100 equiv to benzyl groups of PBLA segment) was diluted with the same volume of NMP, and then the first solution was added and stirred for 4 h at 0 °C (ice bath). The reaction was stopped adding the polymer solution to cold 20% acetic acid (30 mL) drop-by-drop. The neutralized solution was dialyzed against 0.01 M hydrochloric acid solution and then in de-ionized water at 4 °C. As a hydrochloride salt form, a white powder was obtained after lyophilization of the dialyzed solution (91.2 mg, 69.6% yield). The quantitative conversion of the BLA to Asp(DET) was confirmed from the peak intensity ratio of the methylene protons in PEG (–OCH_2CH_2–, δ = 3.7 ppm) to the ethylene protons in the 1,2-diaminoethane moiety ($H_2N(CH_2)_2NH(CH_2)_2NH$–, δ = 2.8–3.4 ppm) in the ^{1}H NMR spectrum in D_2O at 50 °C (Supporting Information).

2.2.2. Synthesis of poly(ethylene glycol)-b-poly{N-[N′-(N″-cis-aconityl-2-aminoethyl)-2-aminoethyl]aspartamide} (PEG-PAsp(DET-Aco))

PEG-PAsp(DET) (17.5 mg, 0.0538 mmol of primary amine) was dissolved in 0.5 M $NaHCO_3$ at pH 9.1 (50 mL). *cis*-Aconitic anhydride powder (420 mg, 2.69 mmol) was added to the solution slowly and stirred at 0 °C for 2 h. The reaction mixture was purified by centrifugal ultrafiltration with Amicon Ultra (MWCO = 10,000; Millipore (Billerica, MA)) three times with de-ionized water at 4 °C. The final product was obtained as a white powder after lyophilization (14.9 mg, 64.7% yield). The quantitative conversion of primary amines in Asp(DET) side chain to *cis*-aconitylamide was confirmed from the peak intensity ratio of the methine protons in the main chain (–$COCH_2CH$(CO–)NH–, –$COCH(CH_2$–)NH–, δ = 4.8 ppm) to methine protons of the *cis*-aconityl moiety (–COCH:C(COONa)CH_2COONa, δ = 6.0 ppm) in ^{1}H NMR spectrum in D_2O at 50 °C (Fig. 1).

2.3. Synthesis of block copolymer with poly(ethylene glycol) and non-charge-conversional polymers (PEG–nCCP) segments

2.3.1. Synthesis of carballylic anhydride

Carballylic anhydride was prepared as previously reported [26] with slight modification. Briefly, tricarballylic acid (4.4 g, 0.025 mol) was reacted with acetic anhydride (4.73 mL, 0.05 mol) at 45 °C for 1 h. The excess of acetic anhydride was evaporated under reduced pressure. Further, the product was dissolved in the minimum amount of ethyl acetate at 80 °C and filtered. The solution was allowed to stand for 5 h at room temperature and then overnight at 4 °C. The obtained crystal was then vacuum-filtered, washed with excess of diethyl ether, and then dried in vacuum to yield a white crystal (760 mg, 19.2% yield). The reaction was confirmed by ^{1}H NMR spectrum in acetone at 25 °C (–$COCH_2CH$(CH_2COOH)CO–, δ = 2.94, 2.86 ppm), (CH_2COOH, δ = 2.44 ppm) (data not shown).

2.3.2. Synthesis of poly(ethylene glycol)-b-poly{N-[N′-(N″-carballylyl-2-aminoethyl)-2-aminoethyl]aspartamide} (PEG-PAsp(DET-Car))

PEG-PAsp(DET) (15 mg, 0.046 mmol of primary amine) was dissolved in 0.5 M $NaHCO_3$ at pH 9.1 (50 mL). Carballylic anhydride powder (Car) (363 mg, 2.3 mmol) was added to the solution slowly and stirred at 0 °C for 2 h. The reaction mixture was purified by centrifugal ultrafiltration with Amicon Ultra (MWCO = 10,000; Millipore (Billerica, MA)) three times with de-ionized water at 4 °C. The final product was obtained as a white powder after lyophilization (13.5 mg, 68.3% yield). The quantitative conversion of the primary amines in the Asp(DET) side chain to carballylylamide was confirmed from the peak intensity ratio of the methine protons in the main chain (–$COCH_2CH$(CO–)NH–, –$COCH(CH_2$–)NH–, δ = 4.8 ppm) to the methylene protons of the carballylyl moiety (–CH_2CH(COONa)CH_2COONa, δ = 2.5) in the ^{1}H NMR spectrum in D_2O at 50 °C (Supporting Information).

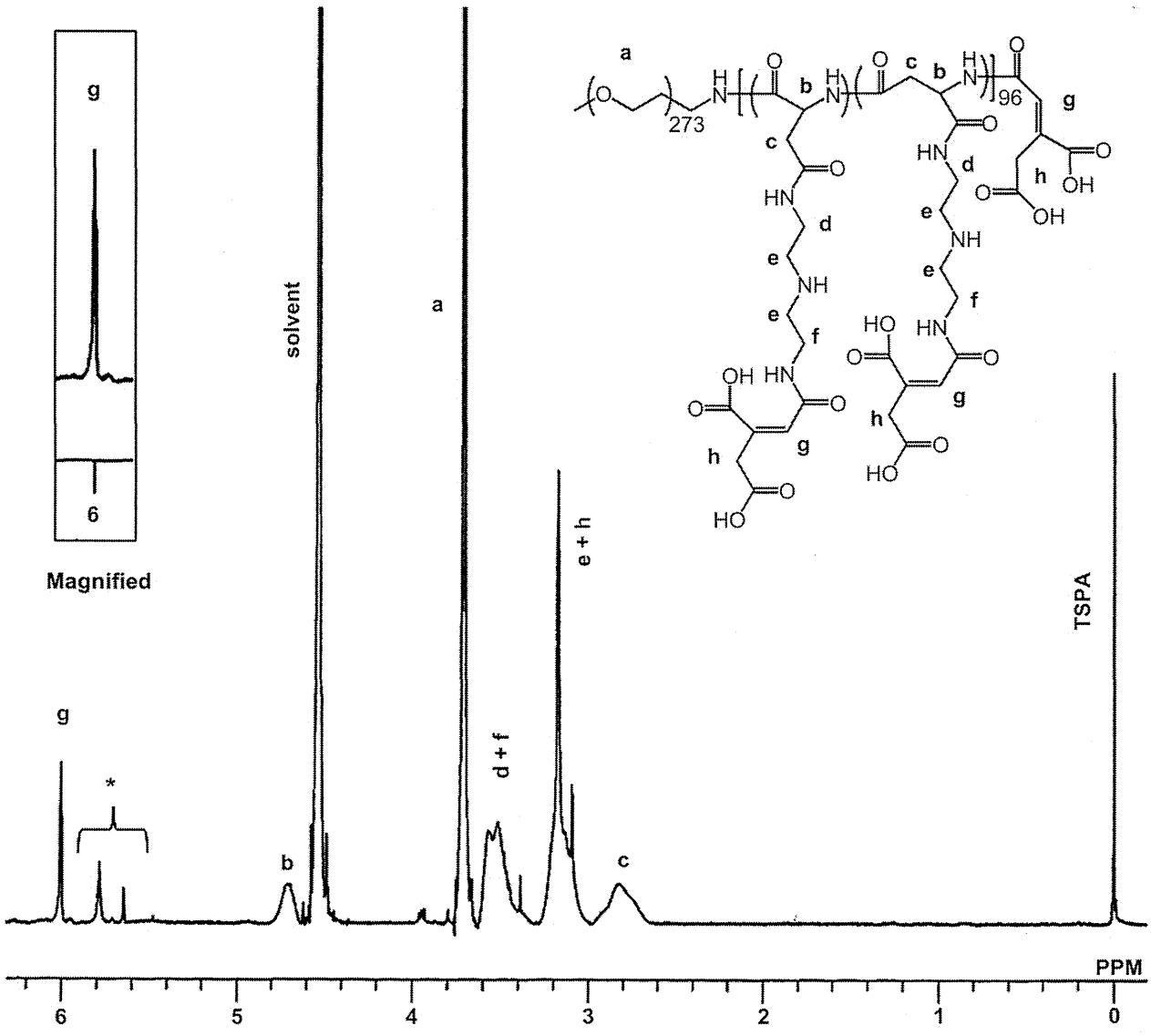

Fig. 1. ^{1}H NMR spectrum of the synthesized PEG-polyanion block copolymer, PEG-PAsp(DET-Aco) (Concentration: 10 mg/mL, Solvent: D_2O, Temperature: 50 °C). *Decarboxilated itaconitylamide (Supporting Information).

2.3.3. Synthesis of poly(ethylene glycol)-b-poly(aspartic acid) (PEG-PAsp)

PEG–PBLA (20 mg, 0.06 mmol) was dissolved in acetonitrile (1.5 mL). Aqueous sodium hydroxide (0.5 N, 6 mL, 50 equiv to benzyl group of PBLA segment) was added to the first solution and allowed to react for 1 h stirring at room temperature. The solution was dialyzed against de-ionized water. A white powder was obtained after lyophilization of the dialyzed solution (18.2 mg, 93.0% yield). The complete deprotection of the flanking benzyl esters in PBLA was confirmed by the peak disappearance of benzyl protons of PBLA ($-CH_2C_6H_5$, $\delta = 7.3$) in the ^{1}H NMR spectrum in D_2O at 50 °C (data not shown).

2.4. Preparation of PEG-polyanion/siRNA/CaP hybrid nanoparticles

A solution of 2.5 M $CaCl_2$ was diluted in 10 mM Tris/HCl buffer (pH 7.5) (1 μL: 11.5 μL). Another solution containing PEG-PAsp(DET-Aco) or PEG-PAsp(DET-Car) (1000 μg/mL) in 10 mM Tris/HCl buffer (pH 7.5) was mixed with a solution of 15 μM siRNA in 10 mM Hepes buffer (pH 7.2) and with 50 mM Hepes buffer containing 1.5 mM Na_3PO_4 and 140 mM NaCl (pH 7.5) (2.5 μL: 5 μL: 5 μL). The former solution was mixed with the latter solution by pipetting for around 20 s (final siRNA concentration; 3 μM). A control nanoparticle containing PEG-PAsp was built as previously described [9]. Each sample solution was used immediately after preparation.

2.5. Dynamic light scattering (DLS)

For the determination of size distribution of hybrid nanoparticles, DLS measurements were carried out at 25 °C using a Zetasizer Nano ZS (Malvern Instruments, UK) at a detection angle of 173° with a He–Ne laser (633 nm) as the incident beam. The data obtained from the rate of decay in the photon correlation function were analyzed with a cumulant method to obtain the corresponding hydrodynamic diameters and polydispersity indices (PdI) (μ/Γ^2) of the nanoparticles.

2.6. Determination of siRNA encapsulated in hybrid nanoparticle

The assay to estimate the amount of siRNA encapsulated in hybrid nanoparticles was carried out as previously reported [11]. Briefly, the sample solutions were centrifuged at 15,000*g* for 30 min to precipitate the nanoparticles. The supernatant was carefully collected to determine the siRNA concentration by measurement of absorbance at 260 nm (Abs_{260}). The percentage of the loaded siRNA was calculated as follows;

Encapsulated percentage (%) = 100 − (Abs_{260} after centrifuge)/(Abs_{260} before centrifuge) × 100

2.7. Transmission electron microscopy (TEM) observation

TEM observation was conducted using H-7000 electron microscope (Hitachi, Tokyo, Japan) operated at 75 kV acceleration voltages. Copper TEM grids with carbon-coated collodion film were glow-discharged for 20 s using an Eiko IB-3 ion coater (Eiko Engineering Co. Ltd., Japan). The grids were dipped into complex solution with 3 μM siRNA, which was mixed with uranyl acetate solution (2% (w/v)), for 30 s. After excess solution was removed using a filter paper, the sample grids were allowed to dry in air and then TEM observation was carried out.

2.8. Cell viability assay

For the cytotoxicity assay, PanC-1 cells (Pancreatic cancer cells, ATCC Number: CRL-1469) were seeded with 100 μL of DMEM containing 10% FBS in a 96 well plate (5000 cells/well) and incubated for 24 h. The nanoparticles (containing 10–1500 nM siRNA) were added with the fresh medium containing 10% FBS, and the cell viability was evaluated after 48-h incubation by Cell Counting Kit-8 (Dojindo, Kumamoto, Japan) according to the protocol provided by the manufacturer. Each well was measured by reading the absorbance at 450 nm in a Microplate Reader (Bio-Rad Model 680, Bio-Rad Laboratories, UK). The results were expressed as the percentage (%) of the control cells, which were incubated only with the culture medium.

2.9. Confocal laser scanning microscopy (CLSM) observation

PanC-1 cells were cultured with 1.5 mL of DMEM containing 10% FBS on 35-mm glass-base dishes (Iwaki, Japan) at 5×10^4 cells/dish. After 24 h, the medium was exchanged with fresh one and Cy5-labeled siRNA-containing nanoparticles were applied to the dish (100 nM siRNA). The nuclei and the endosome/lysosome were stained with Hoechst 33342 (Dojindo Laboratories, Kumamoto, Japan) for 5 min and LysoTracker Green (Molecular Probes, Eugene, OR) for 15 min before CLSM imaging, respectively. Cells were rinsed 3 times with PBS and fresh medium was added prior to the imaging. CLSM images were acquired at 3 and 24 h after nanoparticle administration, using a Zeiss LSM 510 META (Carl Zeiss, Germany) with a water-immersion 63× objective (C-Apochromat, Carl Zeiss). Excitation wavelengths were 488 nm (argon laser), 633 nm (He–Ne laser), and 710 nm (Mai Tai laser, operated in a two-photon mode) for LysoTracker, Cy5, and Hoechst 33342, respectively. The co-localization ratio was calculated as previously described [24] with the formula:

Co-localization ratio = number of yellow pixels/number of yellow and red pixels.

2.10. Real-time reverse transcription (RT)-PCR

PanC-1 cells were seeded with 2000 μL of DMEM containing 10% FBS on a 6 well plate at 8×10^4 cells/well. After 24 h, nanoparticles were added with fresh medium (60 nM siRNA). After 3 h of exposing the cells to nanoparticles, the medium was changed to fresh one. Twenty four hours later, cells were harvested and RNA was extracted using the RNeasy Mini Kit (Qiagen, Valencia, CA), according to the manufacturer's instruction. The amount of extracted RNA was measured and standardized after the genomic DNA elimination for the cDNA synthesis (QuantiTect Reverse Transcription, Quiagen, Valencia, CA). Real-time RT-PCR was performed using the ABI 7500 Fast Real-time RT-PCR System (Applied Biosystems, Foster City, CA) and QuantiTect SYBR Green PCR Master Mix (Qiagen, Valencia, CA). The actin was used as a house-keeper gene and the obtained data were normalized before statistical analysis.

2.11. Statistical analysis

The analysis of variance (ANOVA) was performed to test the treatment effects, and Bonferroni's test was used as *post hoc* pairwise comparisons between individual treatment groups, using the software GraphPad Prism 3.0 (GraphPad Software, Inc.). Statistical significance is represented as * for $p < 0.05$ and ** for $p < 0.01$. Unless indicated, all experiments were performed in triplicate ($N = 3$) and the results reported were expressed as mean values (±SEM).

3. Results and discussion

3.1. Synthesis of charge-conversional and non-charge-conversional polymers

The synthesis route of PEG-PAsp(DET-Aco) as a charge-conversional polyanion is illustrated in Scheme 1, as well as two polyanions used as controls without the charge-conversional property. PEG-PAsp(DET) was synthesized from PEG–PBLA (M_w of PEG 12,000; DP of PBLA 96) by aminolysis reaction with excess of DET molecules. The ^{1}H NMR measurement revealed the quantitative introduction of the *N*-(2-aminoethyl)-2-aminoethyl moiety for successful synthesis of PEG-PAsp(DET) (data not shown). Further, the *cis*-aconityl moiety (Aco) was introduced into the primary amine in the side chain of PAsp(DET) by reacting *cis*-aconitic anhydride with PEG-PAsp(DET) to form an acid-labile *cis*-aconityl-amide in the side chain. The quantitative conversion of primary

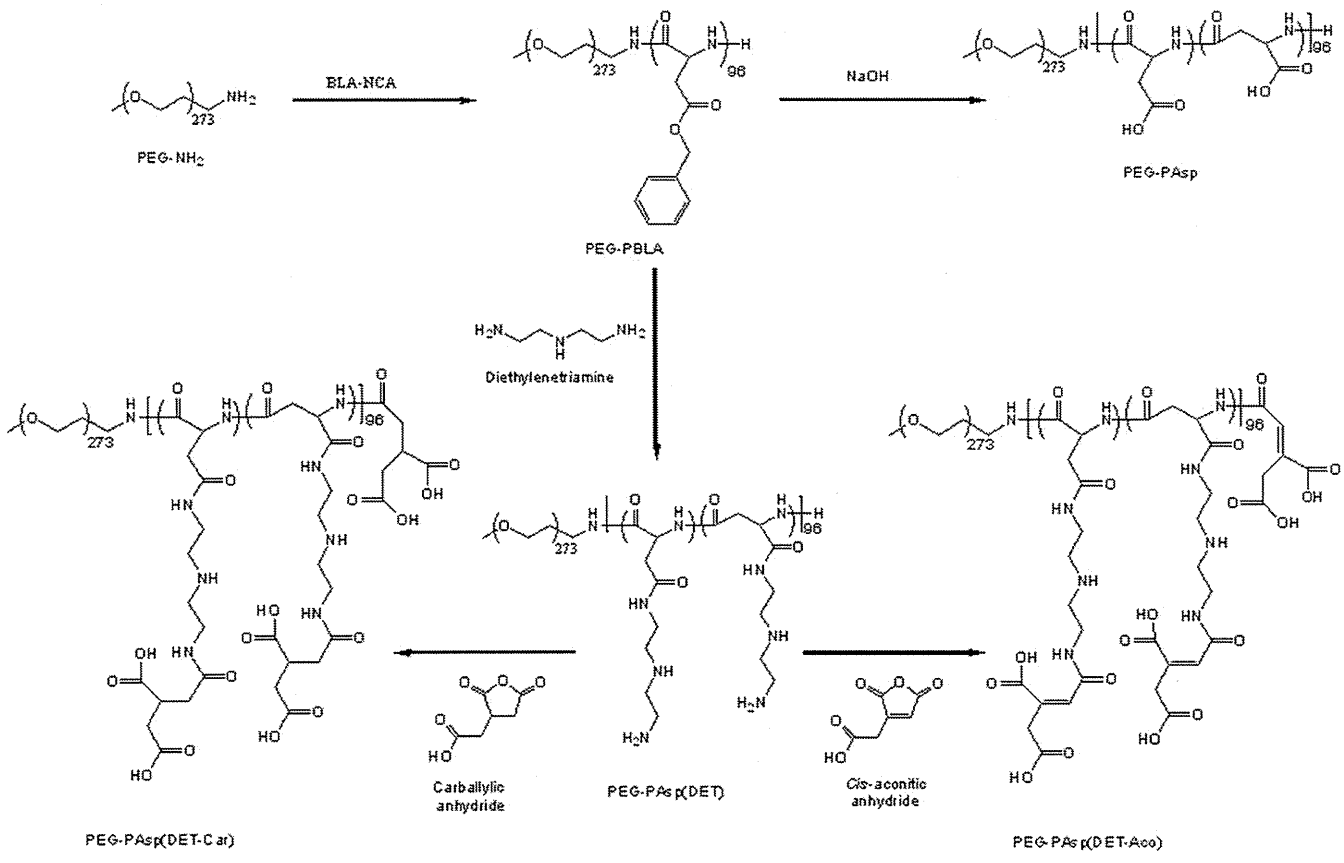

Scheme 1. Synthetic routes of PEG-PAsp(DET-Aco), PEG-PAsp(DET-Car), and PEG-PAsp.

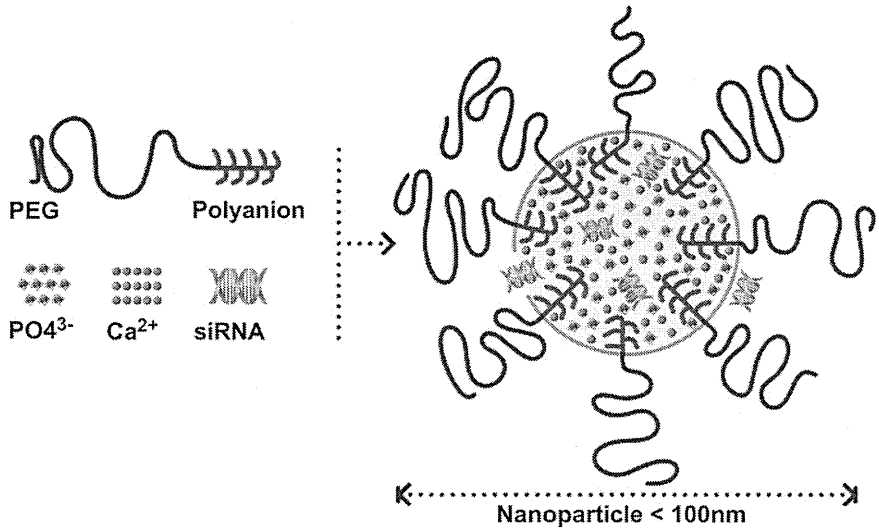

Fig. 2. Schematic illustration of PEG-polyanion/siRNA/CaP hybrid nanoparticles.

amines in Asp(DET) side chain to *cis*-aconitylamide was confirmed from the peak intensity ratio of the methine protons in the main chain to methine protons of the *cis*-aconityl moiety in the ^{1}H NMR spectrum in D_2O (Fig. 1). Although it was also possible to observe the formation of reaction subproducts [27], the desired product of PEG-PAsp(DET-Aco) was obtained in a high ratio (80%). PEG-PAsp (DET-Car) without the acid-labile bond as a control was synthesized by reacting PEG-PAsp(DET) with carballylic anhydride similarly. The quantitative conversion of the primary amines in the Asp(DET) side chain to carballylylamide was confirmed from the peak intensity ratio of the methine protons in the main chain to the methine and methylene protons of carballylyl moiety in the ^{1}H NMR spectrum in D_2O (Supporting Information). In addition, another control polyanion, PEG-PAsp, was prepared by the deprotection of benzyl ester group from PEG–PBLA. The successful deprotection of benzyl ester group was confirmed from the corresponding peak disappearance in the ^{1}H NMR spectrum in D_2O (data not shown). Note that all the reactions were confirmed to proceed without the spontaneous main-chain cleavage [21] from aqueous GPC charts of obtained polymers (data not shown).

3.2. PEG-polyanion/siRNA/CaP hybrid nanoparticle formation and characterization

Great advantages in the utilization of CaP precipitates as a transfection reagent are the fact that they are prepared by a simple and inexpensive method, and also that it efficiently binds/encapsulates polyanions/nucleic acids during the formation process [28,29]. Through self-assembly, CaP nanoparticles containing nucleic acid are formed by the precipitation method in which calcium chloride and phosphate solutions are mixed in the presence of siRNA. However, simple CaP precipitates have potential problems to overcome for efficient nucleic acids delivery; one is the increase in size with time to form large agglomerates in aqueous solutions, and another is poor endosomal escape. To prevent the size increase in CaP precipitates, our previous studies have addressed a preparation of PEG-coated CaP hybrid nanoparticles by mixing of PEG-polyanion block copolymers [9,11–14]. In this study, for further improvement of the PEG-coated CaP nanoparticles, we focused on endosomal escape of the nanoparticles to enhance the gene knockdown efficiency, thus applying a charge-conversional structure PAsp(DET-Aco) [23,24] for the polyanionic segment. Indeed, the hybrid nanoparticles were prepared from the inorganic CaP core, siRNA as a therapeutic payload, and the PEG-PAsp(DET-Aco) as a charge-conversional unit for endosomal escape with minimal cytotoxicity, by mixing calcium and phosphate ionic solutions containing siRNA and the charge-conversional polymer as illustrated in Fig. 2.

The TEM observations with uranyl acetate as a staining agent (Fig. 3A) revealed hybrid nanoparticles with relatively homogenous spherical shape and average size of 42 ± 5 nm. Furthermore, the DLS measurements provided a size histogram in number statistics showing a narrow unimodal distribution with the peak at 38 nm

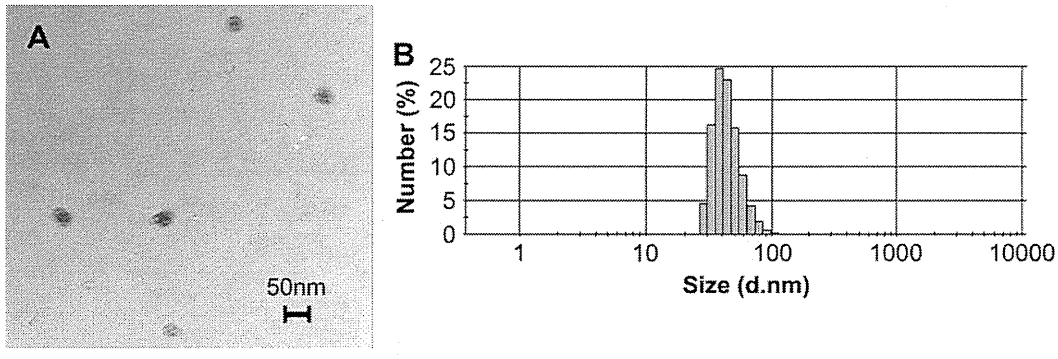

Fig. 3. Size and morphology of PEG-PAsp(DET-Aco)/siRNA/CaP hybrid nanoparticles. A: TEM image (Scale Bar: 50 nm). B: Histogram in number statistics determined by DLS measurement (1 mg/mL PEG-PAsp(DET-Aco) and 3 μM siRNA).

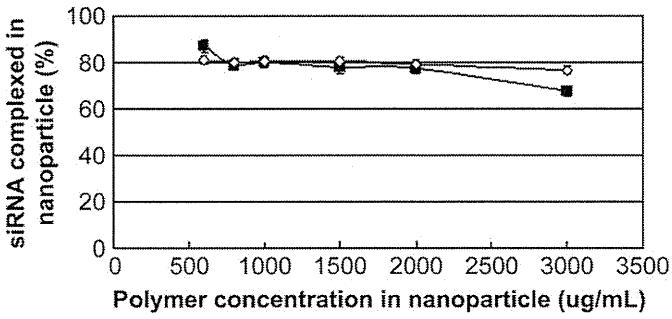

Fig. 4. Percentage of siRNA loaded by the hybrid nanoparticle at varying polymer concentrations (3 μM siRNA). Closed square: PEG-PAsp(DET-Aco), Open diamond: PEG-PAsp(DET-Car).

(Fig. 3B), which was well correlated to the size determined by the TEM observations (Fig. 3A). Samples were confirmed to have the same size even after prolonged incubation time. These results indicate that hybrid nanoparticles can be obtained in a controllable manner using the charge-conversional polymer as colloidal stability agent.

The amount of siRNA encapsulated in the hybrid nanoparticles was monitored against polyanion concentration, determined by the centrifugal assay as previously reported [11]. Effective encapsulation of siRNA in the nanoparticles (around 80%) was confirmed in PEG-PAsp(DET-Aco) concentration between 600 and 2000 μg/mL, while a slight decrease was observed at the concentration of 3000 μg/mL (around 70%) (Fig. 4). Note that the similar binding tendency was observed for the nanoparticle from PEG-PAsp(DET-Car). The siRNA-loading capacities obtained here were close to those found in our previous work with PEG-PAsp (around 85%) [11], indicating efficient entrapment of siRNA by this method regardless of polyanion structures.

3.3. Gene knockdown and cell viability assays

The development of an effective and non-cytotoxic carrier is the main challenge to the success in RNAi therapy. We verified the gene knockdown efficiency of the hybrid nanoparticles to a cultured pancreatic cancer cell (PanC-1) by measuring the level of mRNA. Here, vascular endothelial growth factor (VEGF) was chosen as a target gene because many cancer cells up-regulate VEGF expression to promote angiogenesis, a process characterized by the formation of new blood vessels from a pre-existing vascular network [30,31], facilitating the tumor growth and proliferation. Hence, VEGF knockdown in such cancer cells with siRNA *in vivo* is expected to be a promising strategy to suppress the tumor growth and control cancer evolution (anti-angiogenic therapy).

Hybrid nanoparticles containing 60 nM siVEGF or siLuc as a non-targeted control sequence were applied to PanC-1 cells, and after 3 h of exposure time the medium was replaced and cells were further incubated for 24 h. Thereafter, the real-time RT-PCR analysis was used to determine the mRNA for VEGF. The results revealed that all the tested hybrid nanoparticles with siVEGF possessed potential gene knockdown activity, whereas the nanoparticles with siLuc and naked siVEGF showed no gene knockdown (Fig. 5), indicating the siVEGF sequence-specific gene knockdown with the hybrid nanoparticles. Among them, the nanoparticle from PEG-PAsp(DET-Aco) presented the only significant and highest gene knockdown (~82%). The comparison of PEG-PAsp(DET-Aco) with the other PEG-polyanions strongly suggests that the acid-labile *cis*-aconitylamide in PEG-PAsp(DET-Aco) should be essential for the significant gene knockdown. Next, the cytotoxicity of the hybrid nanoparticles was evaluated to PanC-1 cells. A wide range of siRNA concentration was tested from 10 to 1500 nM along with the increase in all the other components. As shown in Fig. 6, no significant cytotoxicity was observed for both hybrid nanoparticles from PEG-PAsp(DET-Aco/Car) even at the highest concentration (50 μg/mL PEG-polyanion, 1.5 μM siRNA). From these results, we concluded that the hybrid nanoparticles from PEG-PAsp(DET-Aco) allowed efficient siRNA delivery into the cytoplasm of cultured PanC-1 with negligible cytotoxicity.

3.4. Cellular uptake and intracellular trafficking

In siRNA transfection process, after cellular internalization as the first hurdle, siRNA carriers will be delivered to early endosomes,

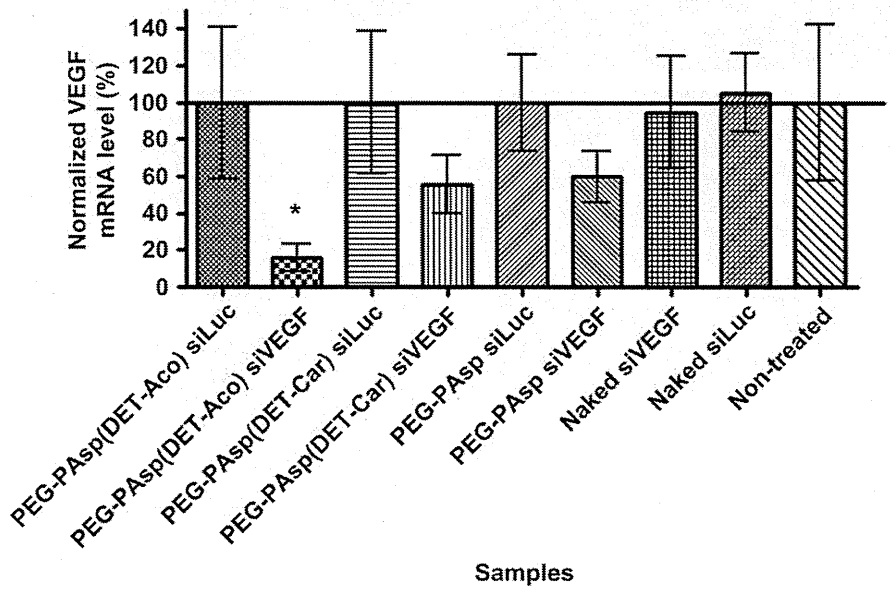

Fig. 5. Gene knockdown in PanC-1 at 24 h after 3 h of nanoparticles exposition to cells (60 nM siRNA, $N = 9$). Controls were set as 100%. *$p < 0.05$ comparing to controls (ANOVA followed by Bonferroni).

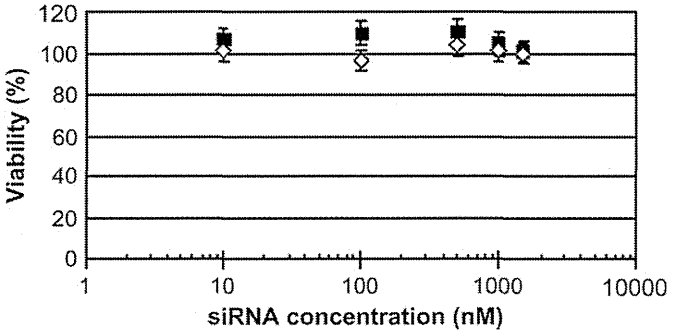

Fig. 6. Cell viability of PanC-1 cells incubated with hybrid nanoparticles for 48 h ($N = 6$). siLuc concentration was changed from 10 to 1500 nM, corresponding to the polymer concentration from 0.7 to 50 μg/mL. Closed square: PEG-PAsp(DET-Aco), Open diamond: PEG-PAsp(DET-Car).

followed by the movement to late endosomes/lysosomes for siRNA degradation [6]. Thus, the smooth endosomal escape is a critical requirement for the effective gene silencing with siRNA. In the preceding section, the utility of PEG-PAsp(DET-Aco) was demonstrated for significant VEGF mRNA knockdown without marked cytotoxicity. Here, we verified whether the excellent gene knockdown is attributed to endosomal escape with PEG-PAsp(DET-Aco) along with our initial hypothesis. Accordingly, we observed the intracellular trafficking of each hybrid nanoparticle after 3- and 24-h incubation with PanC-1 cells. In the obtained images, Cy5-siRNA, endosomes/lysosomes, and nuclei were shown in red, green, and blue, respectively, and thus yellow pixels result in the merge of red and green pixels, indicating the co-localization of Cy5-siRNA with endosome/lysosome. The images of PanC-1 cells treated with PEG-PAsp(DET-Aco)/PEG-PAsp(DET-Car) nanoparticles displayed red and/or yellow regions with 3-h incubation (Fig. 7A and B), indicating that both of the nanoparticles allowed the significant cellular uptake of Cy5-siRNA. In these two images, only the nanoparticles containing PEG-PAsp(DET-Aco) in the formulation presented widely extended red regions in cells (Fig. 7A), corresponding to the presence of Cy5-siRNA in the cytoplasm. In contrast, the cells treated with the other nanoparticles containing PEG-PAsp(DET-Car) mainly displayed perinuclear yellow spots (Fig. 7B), indicating the endosomal/lysosomal capture of Cy5-siRNA. These results are well consistent with our hypothesis that the integration of PEG-PAsp(DET-Aco) into the nanoparticles intensely facilitates the endosomal escape of the hybrid nanoparticles in the early stage of transfection, presumably due to the charge-conversional property

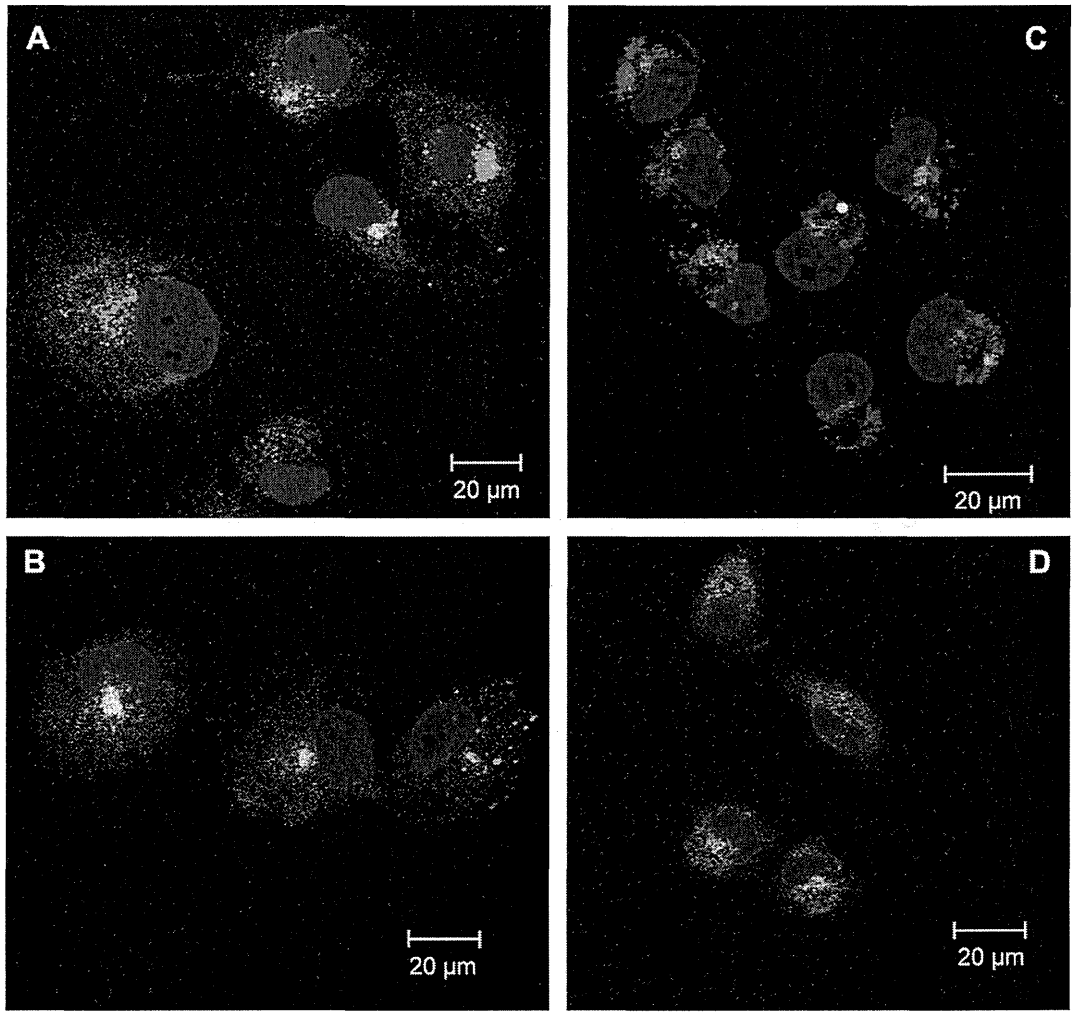

Fig. 7. Confocal laser scanning microscopic observation for intracellular trafficking of hybrid nanoparticles. Images were taken at 3 and 24 h after nanoparticle application. A: PEG-PAsp(DET-Aco), B: PEG-PAsp(DET-Car) nanoparticles incubated for 3 h (100 nM siRNA). C: PEG-PAsp(DET-Aco), D: PEG-PAsp(DET-Car) nanoparticles incubated for 24 h (100 nM siRNA). Blue: Hoechst at 710 nm (two-photon excitation); Green: Lysotracker at 488 nm; and Red: Cy5 at 633 nm.

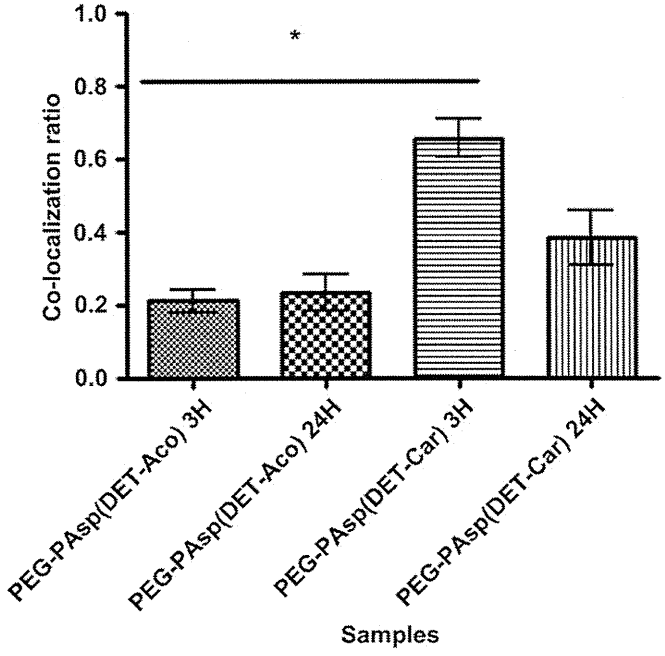

Fig. 8. Co-localization ratio of Cy5-labeled siRNA with endosome/lysosome obtained by analyzing the images. Results were expressed as mean ± SEM (from three cells) (*$p < 0.01$).

to reproduce the endosomal membrane destabilizing polycation, PAsp(DET), in the acidic endocytic vesicles. On the other hand, after 24-h incubation, the cells treated with PEG-PAsp(DET-Car) nanoparticles obviously increased red regions (Fig. 7D), suggesting that the hybrid nanoparticles might originally have an endosomal escaping ability apart from the charge-conversional polymers. A possible explanation of this delayed endosomal escape is that CaP core disassembles under a low ionic condition in endocytic vesicles for increased-ion induced-osmotic pressure to induce endosomal membrane disruption [11], similar to the proton sponge hypothesis known to polyethyleneimine [32]. Eventually, the co-localization of Cy5-siRNA with endosome/lysosome was quantitatively analyzed for PEG-PAsp(DET-Aco) and PEG-PAsp(DET-Car), as summarized in Fig. 8. The obtained tendency in endosomal escape of each nanoparticle is well correlated with the result in the gene knockdown experiment (Fig. 5). Earlier endosomal escape of siRNA by PEG-PAsp (DET-Aco) probably leads to more efficient gene knockdown with the nanoparticles.

4. Conclusion

This work was aimed to develop a hybrid nanocarrier system consisting of CaP and the PEG–charge-conversional polymer for safe and efficient siRNA delivery. To improve the endosomal escape of the nanoparticles, we integrated the charge-conversional polymer PEG-PAsp(DET-Aco) into the nanoparticles, in which PEG-PAsp (DET-Aco) induces the destabilization of endosomal membrane by producing a polycation PAsp(DET) via the selective cleavage of *cis*-aconitylamide in acidic endosome/lysosome. The size less than 100 nm with narrow size distribution and a high siRNA-loading capacity were confirmed for PEG-PAsp(DET-Aco)/siRNA/CaP nanoparticles, which achieved strong VEGF knockdown to PanC-1 with negligible cytotoxicity through the rapid endosomal escape. These findings demonstrate our hybrid system as a promising candidate to future *in vivo* siRNA applications for pancreatic cancer treatment based on anti-angiogenic therapy.

Acknowledgments

This research is supported by the Japan Society for the Promotion of Science (JSPS) through its "Funding Program for World-Leading Innovative R&D on Science and Technology (FIRST Program)". F.P. acknowledges the fellowship from Ministry of Education, Science, Sports and Culture, Japan (MEXT).

Appendix

Figures with essential color discrimination. Figs. 2, 3 and 7 in this article are difficult to interpret in black and white. The full color images can be found in the online version, at doi:10.1016/j.biomaterials.2010.12.057.

Appendix. Supporting information

Supplementary data associated with this article can be found, in the online version, at doi:10.1016/j.biomaterials.2010.12.057.

References

[1] Fire A, Xu S, Montgomery MK, Kostas SA, Driver SE, Mello CC. Potent and specific genetic interference by double-stranded RNA in *Caenorhabditis elegans*. Nature 1998;391:806–11.
[2] Elbashir SM, Harborth J, Lendeckel W, Yalcin A, Weber K, Tuschl T. Duplexes of 21-nucleotide RNAs mediate RNA interference in cultured mammalian cells. Nature 2001;411:494–8.
[3] International Human Genome Sequencing Consortium. Initial sequencing and analysis of the human genome. Nature 2001;409:860–921.
[4] Venter JC, Adams MD, Myers EW, Li PW, Mural RJ, Sutton GG, et al. The sequence of the human genome. Science 2001;291:1304–51.
[5] International Human Genome Sequencing Consortium. Finishing the euchromatic sequence of the human genome. Nature 2004;431:931–45.
[6] Whitehead KA, Langer R, Anderson DG. Knocking down barriers: advances in siRNA delivery. Nat Rev Drug Discov 2009;8(2):129–38.
[7] Graham FL, van der Eb AJ. A new technique for the assay of infectivity of human adenovirus 5 DNA. Virology 1973;52:456–67.
[8] Jordan M, Schallhorn A, Wurm FM. Transfecting mammalian cells: optimization of critical parameters affecting calcium–phosphate precipitate formation. Nucleic Acids Res 1996;24:596–601.
[9] Kakizawa Y, Kataoka K. Block copolymer self-assembly into monodispersive nanoparticles with hybrid core of antisense DNA and calcium phosphate. Langmuir 2002;18:4539–43.
[10] Maitra A. Calcium phosphate nanoparticles: second-generation nonviral vectors in gene therapy. Expert Rev Mol Diagn 2005;5(6):893–905.
[11] Kakizawa Y, Furukawa S, Kataoka K. Block copolymer-coated calcium phosphate nanoparticles sensing intracellular environment for oligodeoxynucleotide and siRNA delivery. J Control Release 2004;97:345–56.
[12] Kakizawa Y, Miyata K, Furukawa S, Kataoka K. Size-controlled formation of a calcium phosphate-based organic-inorganic hybrid vector for gene delivery using poly(ethylene glycol)-*block*-poly(aspartic acid). Adv Mater 2004;16 (8):699–702.
[13] Kakizawa Y, Furukawa S, Ishii A, Kataoka K. Organic–inorganic hybrid-nanocarrier of siRNA constructing through the self-assembly of calcium phosphate and PEG-based block aniomer. J Control Release 2006;111:368–70.
[14] Zhang MZ, Ishii A, Nishiyama N, Matsumoto S, Ishii T, Yamasaki Y, et al. PEGylated calcium phosphate nanocomposites as smart environment-sensitive carriers for siRNA delivery. Adv Mater 2009;21(34):3520–5.
[15] Francis G, Delgado C, Fisher D, Malik F, Agrawal AK. Polyethylene glycol modification: relevance to improved methodology to tumour targeting. J Drug Target 1996;3:321–40.
[16] Monfardini C, Veronese FM. Stabilization of substances in the circulation. Bioconjug Chem 1998;9:418–50.
[17] Kataoka K, Harada A, Nagasaki Y. Block copolymer micelles for drug delivery: design, characterization and biological significance. Adv Drug Deliv Rev 2001;47:113–31.
[18] Dominska M, Dykxhoorn DM. Breaking down the barriers: siRNA delivery and endosome escape. J Cell Sci 2010;123:1183–9.
[19] Kanayama N, Fukushima S, Nishiyama N, Itaka K, Jang W-D, Miyata K, et al. A PEG-based biocompatible block catiomer with high buffering capacity for the construction of polyplex micelles showing efficient gene transfer toward primary cells. ChemMedChem 2006;1:439–44.
[20] Miyata K, Oba M, Nakanishi M, Fukushima S, Yamasaki Y, Koyama H, et al. Polyplexes from poly(aspartamide) bearing 1,2-diaminoethane side chains induce pH-selective, endosomal membrane destabilization with amplified transfection and negligible cytotoxicity. J Am Chem Soc 2008;130(48): 16287–94.

[21] Itaka K, Ishii T, Hasegawa Y, Kataoka K. Biodegradable polyamino acid-based polycations as safe and effective gene carrier minimizing cumulative toxicity. Biomaterials 2010;31(13):3707–14.
[22] Kim HJ, Ishii A, Miyata K, Lee Y, Wu S, Oba M, et al. Introduction of stearoyl moieties into a biocompatible cationic polyaspartamide derivative, PAsp (DET), with endosomal escaping function for enhanced siRNA-mediated gene knockdown. J Control Release 2010;145(2):141–8.
[23] Lee Y, Miyata K, Oba M, Ishii T, Fukushima S, Han M, et al. Charge conversion ternary polyplex with endosomes disruption moiety: a technique for efficient and safe gene delivery. Angew Chem Int Ed Engl 2008;120:5241–4.
[24] Sanjoh M, Hiki S, Lee Y, Oba M, Miyata K, Ishii T, et al. pDNA/poly(l-lysine) polyplexes functionalized with a pH-sensitive charge-conversional poly (aspartamide) derivative for controlled gene delivery to human umbilical vein endothelial cells. Macromol Rapid Commun 2010;31(13):1181–6.
[25] Lee Y, Fukushima S, Bae Y, Hiki S, Ishii T, Kataoka K. A protein nanocarrier from charge-conversion polymer in response to endosomal pH. J Am Chem Soc 2007;129:5362–3.
[26] Elgazwy A-SSH. Facile synthesis of (*R*, *R*) and of (*R*, *S*) tricarballylic acid anhydride and imide derivatives. Molecules 2000;5:665–73.
[27] Dinand E, Zloh M, Brocchini S. Competitive reactions during amine addition to *cis*-aconityl anhydride. Aust J Chem 2002;55:467–74.
[28] Sokolova VV, Radtke I, Heumann R, Epple M. Effective transfection of cells with multi-shell calcium phosphate–DNA nanoparticles. Biomaterials 2006;27:3147–53.
[29] Zhang M, Kataoka K. Nano-structured composites based on calcium phosphate for cellular delivery of therapeutic and diagnostic agents. Nano Today 2009;4:508–17.
[30] Sullivan LA, Brekken RA. The VEGF family in cancer and antibody-based strategies for their inhibition. MAbs 2010;2(2):165–75.
[31] Dvorak HF. Vascular permeability factor/vascular endothelial growth factor: a critical cytokine in tumor angiogenesis and a potential target for diagnosis and therapy. J Clin Oncol 2002;20:4368–80.
[32] Boussif O, Lezoualc'h F, Zanta MA, Mergny MD, Scherman D, Demeneix B, et al. A versatile vector for gene and oligonucleotide transfer into cells in culture and *in vivo*: polyethylenimine. Proc Natl Acad Sci U S A 1995;92:7297–301.

EXPERT OPINION

informa
healthcare

Short interfering RNA and the central nervous system: development of nonviral delivery systems

Kazutaka Nishina, Hidehiro Mizusawa & Takanori Yokota†
Tokyo Medical and Dental University, Graduate School, Department of Neurology and Neurological Science, Tokyo, Japan

The development of gene silencing therapies for neurological diseases has placed great importance on the delivery of short interfering RNA (siRNA) to the central nervous system (CNS). However, delivery of siRNA to neurons, glia and brain capillary endothelial cells (BCECs) has not been well established. This editorial describes different approaches that are being used to efficiently deliver siRNA to the CNS via intravenous, intracerebroventricular, or intranasal administration.

Keywords: central nervous system, intracerebroventricular administration, intranasal administration, intravenous administration, siRNA delivery

Expert Opin. Drug Deliv. (2013) 10(3):289-292

1. Introduction

Because no disease-modifying therapies are currently available to treat neurodegenerative diseases, such as Alzheimer's disease, Parkinson's disease, Huntington's disease and amyotrophic lateral sclerosis, silencing the causative gene using short interfering RNA (siRNA) is a promising method for treating these diseases. However, it is technically challenging to deliver siRNA to the central nervous system (CNS) because of the blood–brain barrier (BBB). The BBB is composed mainly of brain capillary endothelial cells (BCECs), pericytes and astrocyte foot processes. The BBB is both a physical barrier, resulting from the presence of endothelial tight junctions, and a transport barrier, resulting from the presence of selective membrane transporters and vesicular trafficking via BCECs. To cross the BBB, moieties must have a molecular weight of < 500 Da and be lipophilic [1]; siRNAs, however, have a molecular weight of > 14,000 Da and are hydrophilic. Improved delivery systems are therefore necessary to achieve effective gene silencing therapy in the CNS. Recently, several methods of delivering siRNAs to the CNS were developed. These methods include the use of hydrodynamic injection technique, conjugation of the siRNA to a lipid or peptide and the use of nanoparticles. The siRNAs were then administered through the intravenous (i.v.), intracerebroventricular (ICV), or intranasal (IN) routes. This editorial focuses on recent progress of administration to the CNS (**Table 1**).

2. Intravenous administration

A few reports have successfully delivered siRNA into the brain across the BBB [2-5]. At first, there are few reports using liposomes conjugated with peptidomimetic monoclonal antibody that bind to specific endogenous receptors (i.e., insulin and transferrin receptors) located on both the BBB and the brain cellular membranes [2].

10.1517/17425247.2013.748746 © 2013 Informa UK, Ltd. ISSN 1742-5247, e-ISSN 1744-7593

Table 1. Advantages and disadvantages of each administration route.

	Advantages	Disadvantages
i.v.	Be able to target whole brain including BBB	Difficult to pass through the BBB
ICV	Highly effective	Highly invasive
IN	Easiest and safest route of administration	Insufficient effect

Recent reports used the same short peptide derived from rabies viral glycoprotein (RVG) [3-5]. RVG interacts specifically with the nicotinic acetylcholine receptor (AChR) on neuronal cells to enable viral entry into the cells [3]. The nine-arginine-conjugated RVG peptide (RVG-9R) binds to negatively charged siRNA and can deliver siRNA to neural cells after i.v. administration [3]. This method has been used to specifically deliver siRNA to CNS cells, where it successfully inhibited the target endogenous gene [3]. The i.v. administration of RVG-9R was also used to target delivery of the siRNA to macrophages and microglial cells in the CNS [4]. Recently, i.v. administrated RVG-fused exosomes, which are endogenous nanovesicles that can transport materials including miRNA, were used in delivering siRNA specifically to neurons, microglia and oligodendrocytes in the brain, where it reduced the expression of an endogenous target gene [5]. Using siRNA-RVG exosome, no significant elevations of cytokines including IL-6, TNF-α and IFN-α were registered in contrast to siRNA-RVG-9R, which potently stimulated IL-6 secretion [5]. The mechanism by which RVG transverses the BBB is still not clear, but using RVG is a promising method for delivering siRNA across the BBB to the brain after i.v. administration.

Another drug delivery system to the neuron using i.v. administration, MRI-guided focused ultrasound (MRIgFUS), combined with intravascular delivery of microbubble contrast agent, was reported [6]. MRIgFUS was noninvasive delivery system of cholesterol-conjugated siRNA to CNS and was used to locally and transiently disrupt the BBB [6].

The BCECs are no longer regarded as an inert vascular lining that is injured and morphologically changed during the infarction, but are now understood to actively play many important roles in the pathophysiological mechanisms of ischemia, inflammation and transport across the BBB. Thus, gene silencing therapy in the BBB is being considered for the treatment of major neurological diseases, such as brain ischemia, multiple sclerosis and Alzheimer's disease. We first reported the delivery of siRNA into BCECs using a hydrodynamic injection technique [7]. However, hydrodynamic injection cannot be applied clinically because of the volume overload and extremely high hydrostatic pressure involved. Next, we reported the efficient delivery of siRNA into BCECs using an endogenous lipoprotein [8]. We chose to conjugate cholesterol to the siRNA for incorporation into extracted endogenous high-density lipoproteins (HDL), because cholesterol can be endocytosed via HDL receptors expressed in BCECs, but cannot enter the brain. Cholesterol-conjugated siRNA was successfully delivered into BCECs by receptor-mediated uptake and suppressed an endogenous gene in BCECs.

3. Intracerebroventricular administration

ICV administration can be used to bypass the BBB and other mechanisms that limit drug distribution into the brain [9]. Gene silencing using ICV administration of siRNA has been reported [10-12]. The ICV infusion of naked siRNA into the third ventricle of the mouse brain suppressed a target gene at a dose of 3 μmol [10], but another study showed that naked siRNA does not reach brain cells as well as naked antisense oligonucleotide after ICV administration [11]. To increase the stability and efficiency of siRNA, several chemical modifications ('Accell siRNA') have been introduced into siRNA nucleotides. Although its mechanism of delivery is unknown, chemically modified siRNA reduced expression of target genes in neurons, but not glia, after ICV administration [12]. These results suggest that chemical modification is necessary to deliver siRNA to the CNS even when using ICV administration.

We reported efficient siRNA delivery by ICV administration when using lipoprotein as an *in vivo* carrier for the siRNA [13]. We used α-tocopherol-conjugated siRNA to bind serum HDL, and we achieved dramatic improvement in siRNA delivery to neurons. In brain, α-tocopherol is incorporated into HDL-like particles that are synthesized in astrocytes and transferred to neurons and glial cells. Serum HDL and HDL-like particles have similar particle size and density and both use apolipoprotein E as a ligand for receptors. The dose of unconjugated siRNA needed for target suppression was as much as 3 μmol [9], whereas we found that only 3 nmol of α-tocopherol-conjugated siRNA with HDL could inhibit a target gene to a comparable degree [13].

Recently, the study showed chemically modified single-stranded siRNAs (ss-siRNAs) dramatically improve both potency and activity to treat model mouse of Huntington's disease by ICV administration [14]. The ss-siRNAs activity required chemical modifications including phosphorothioate linkages, 2′-methoxyribose, 2′-fluororibose, 2′-methoxyethyl-ribose, and 5-(*E*)-vinylphosphonate. The ss-siRNAs do not require special formulations to distribute to peripheral tissues, and it is very useful to clinical application.

4. Intranasal administration

IN administration is a noninvasive method of drug delivery that may also bypass the BBB to allow therapeutic substances, including siRNA, to cross to the CNS. The advantage of this method is the rapid onset of effects without injection. The

disadvantage of this route is that the limited absorption across the nasal epithelium has restricted its application to particularly potent substances [15].

One recent study examined the delivery of the chemically modified siRNA from the nasal cavity to the olfactory bulbs via the olfactory nerve pathway [16]. The chemically modified siRNA was delivered to the olfactory bulbs via the olfactory nerve but was not distributed to other regions of the brain [16]. Other studies of IN administration of siRNA using dendrimers [17,18] showed more efficient delivery of siRNA to additional brain regions, including the hypothalamus, amygdala, cerebral cortex and striatum [17]. IN administration of siRNA using e-PAM-R, a biodegradable poly(amidoamine) dendrimer, as a carrier reduced expression of the target gene *HMGB1* in the prefrontal cortex and striatum, and also suppressed infarct volume in the postischemic rat brain [17]. Another study that used poly (amidoamine) G7 dendrimers complexed with ^{32}P-labeled siRNA achieved higher brain radioactivity than that achieved by i.v. injection of dendriplexes or IN administration of naked siRNA [18]. These results indicate that the IN delivery of siRNAs complexed with dendrimers may be an efficient method of gene suppression therapy in the restricted area of the CNS.

5. Conclusion

Gene suppression using siRNA is a promising approach for treating neurodegenerative diseases. Several methods have shown efficacy in animal models, but further increase in the efficiency of delivery is needed.

6. Expert opinion

The use of siRNA as therapy for CNS disorders is currently under investigation, but getting siRNAs to cross the BBB and to be sufficiently available in the CNS upon systemic administration remains difficult. Each delivery route, i.v., ICV or IN, has advantages and disadvantages. The i.v. method is the most common administration route clinically, but it is still a big challenge to get the large, polar siRNA molecules to pass through the BBB. The ICV method more effectively suppresses target genes than the other routes, but it is invasive. The IN method is the easiest and safest route of administration, and it affords an opportunity for repeated self-administration, but its silencing effect is still weak.

In conclusion, these novel protocols we described are likely to be useful not only in experimental investigations but also in the clinical application of siRNA in the treatment of CNS disorders. Another useful chemical modification, conjugation of usable molecule, or using practical nanoparticle will be needed in order for siRNA to be used clinically in the CNS. Although further developments of these items are required, siRNA delivery strategies to the CNS are being used more widely, and we think that these methods should make treating CNS disorders possible.

Declaration of interest

This study was supported by grants from the National Institute of Biomedical Innovation, Japan (to T Yokota) and the Ministry of Health, Labor and Welfare, Japan (to T Yokota and H Mizusawa). The authors state no conflict of interest and have received no payment in preparation of this manuscript.

Bibliography

Papers of special note have been highlighted as either of interest (•) or of considerable interest (••) to readers.

1. Barchet TM, Amiji MM. Challenges and opportunities in CNS delivery of therapeutics for neurodegenerative diseases. Expert Opin Drug Deliv 2009;6(3):211-25
2. Boado RJ. Blood–brain barrier transport of non-viral gene and RNAi therapeutics. Pharm Res 2007;24(9):1772-87
3. Kumar P, Wu H, McBride JL, et al. Transvascular delivery of small interfering RNA to the central nervous system. Nature 2007;448(7149):39-43

•• **The first paper reporting transvascular delivery of siRNA to the CNS.**

4. Kim SS, Ye C, Kumar P, et al. Targeted delivery of siRNA to macrophages for anti-inflammatory treatment. Mol Ther 2010;18(5):993-1001
5. Alvarez-Erviti L, Seow Y, Yin H, et al. Delivery of siRNA to the mouse brain by systemic injection of targeted exosomes. Nat Biotechnol 2011;29(4):341-5

• **Use of RVG-fused exosomes to deliver siRNA across the BBB.**

6. Burgess A, Huang Y, Querbes W, et al. Focused ultrasound for targeted delivery of siRNA and efficient knockdown of Htt expression. J Control Release 2012;163(2):125-9
7. Hino T, Yokota T, Ito S, et al. In vivo delivery of small interfering RNA targeting brain capillary endothelial cells. Biochem Biophys Res Commun 2006;340(1):263-7
8. Kuwahara H, Nishina K, Yoshida K, et al. Efficient in vivo delivery of siRNA into brain capillary endothelial cells along with endogenous lipoprotein. Mol Ther 2011;19(12):2213-21

•• **The first report of siRNA delivery into BCECs using cholesterol-conjugated siRNA considerable clinical usage.**

9. Cook AM, Mieure KD, Owen RD, et al. Intracerebroventricular administration of drugs. Pharmacotherapy 2009;29(7):832-45
10. Thakker DR, Natt F, Hüsken D, et al. Neurochemical and behavioral consequences of widespread gene knockdown in the adult mouse brain by using nonviral RNA interference. Proc Natl Acad Sci USA 2004;101(49):17270-5

• **The first report of efficient ICV administration of siRNA.**

11. Senn C, Hangartner C, Moes S, et al. Central administration of small interfering RNAs in rats: a comparison with antisense oligonucleotides. Eur J Pharmacol 2005;522(1-3):30-7
12. Nakajima H, Kubo T, Semi Y, et al. A rapid, neuron-selective, in vivo knockdown following a single intracerebroventricular injection of a novel chemically modified siRNA in the adult rat brain. J Biotechnol 2012;157(2):326-33
13. Uno Y, Piao W, Miyata K, et al. High-density lipoprotein facilitates in vivo delivery of alpha-tocopherol-conjugated short-interfering RNA to the brain. Hum Gene Ther 2011;22(6):711-19

•• **ICV administration of α-tocopherol-conjugated siRNA is a highly efficient method of siRNA delivery.**

14. Yu D, Pendergraff H, Liu J, et al. Single-Stranded RNAs use RNAi to potently and allele-selectively inhibit mutant Huntingtin expression. Cell 2012;150(5):895-908

•• **The first report of efficient ICV administration of single-stranded siRNA.**

15. Lochhead JJ, Thorne RG. Intranasal delivery of biologics to the central nervous system. Adv Drug Deliv Rev 2012;64(7):614-28
16. Renner DB, Frey WH II, Hanson LR. Intranasal delivery of siRNA to the olfactory bulbs of mice via the olfactory nerve pathway. Neurosci Lett 2012;513(2):193-7
17. Kim ID, Shin JH, Kim SW, et al. Intranasal delivery of HMGB1 siRNA confers target gene knockdown and robust neuroprotection in the postischemic brain. Mol Ther 2012;20(4):829-39

•• **IN administration of siRNA dendriplexes is also an efficient siRNA delivery method.**

18. Perez AP, Mundiña-Weilenmann C, Romero EL, et al. Increased brain radioactivity by intranasal ^{32}P-labeled siRNA dendriplexes within in situ-forming mucoadhesive gels. Int J Nanomedicine 2012;7:1373-85

Affiliation

Kazutaka Nishina[1] MD PhD,
Hidehiro Mizusawa[2] MD PhD &
Takanori Yokota[†2] MD PhD
[†]Author for correspondence
[1]Medical Fellow,
Tokyo Medical and Dental University,
Graduate School,
Department of Neurology and Neurological Science,
1-5-45, Yushima, Bunkyo-ku,
Tokyo 113-8519, Japan
[2]Professor,
Tokyo Medical and Dental University,
Graduate School,
Department of Neurology and Neurological Science,
1-5-45, Yushima, Bunkyo-ku,
Tokyo 113-8519, Japan
Tel: +81 3 5803 5234;
Fax: +81 3 5803 0169;
E-mail: tak-yokota.nuro@tmd.ac.jp